Contents

Chapter 1

Theory

1.1 Higgs Phenomenology

The Higgs sector of the Minimal Supersymmetric Standard Model (MSSM) consists of two SU (2) dou- blets, H1 and H2 , whose relative contribution to electroweak symmetry breaking is determined by the ratio of vacuum expectation values of their neutral components, tan   v2 /v1 . The spectrum of phys- ical Higgs bosons is richer than in the SM, consisting of two neutral scalars h and H, one neutral pseu- doscalar, A, and two charged scalars, H. At the tree level, the mass matrix for the neutral scalars can be expressed in terms of the parameters MZ , MA and tan , and the mass of the lightest scalar h is bounded from above by MZ . However, radiative corrections especially those involving top and bottom quarks and their supersymmetric partners, the stop and sbottom squarks can significantly alter the tree-level predictions for the Higgs-boson masses, and bring along a dependence on a large number of free pa- rameters of the MSSM. While the CP symmetry is conserved at tree level in the MSSM Higgs sector, radiative corrections can also introduce CP-violating phases, and induce mixing among all three neutral states. In this report, however, we will focus on the CP-conserving case, by considering only real values for the parameters in the soft SUSY-breaking Lagrangian and for the Higgs mass in the superpotential. In general, the couplings of the MSSM Higgs bosons to gauge bosons and matter fermions dif- fer from those of the SM Higgs. However, in large regions of the MSSM parameter space one of the scalars has SM-like couplings, while the other Higgs bosons are decoupled from the gauge bosons, and their couplings to down-type (up-type) fermions are enhanced (suppressed) by tan . As in the SM, gluon fusion is one of the most important production mecha- nisms for the neutral Higgs bosons, whose couplings to the gluons are mediated by the top and bottom quarks and their superpartners. However, for intermediate to large values of tan the associated production with bottom quarks can become the dominant production mechanism for the neutral Higgs bosons that have enhanced couplings to down- type fermions. The production of the charged Higgs H, on the other hand, proceeds mainly through its coupling to a top-bottom pair. A suffi- ciently light H is produced in the decay of a top quark, and it decays dominantly in a tau-neutrino pair. A heavy H is produced in association with a top quark and it decays dominantly in a top-bottom pair. The discovery by ATLAS and CMS of

what appears to be a neutral scalar with mass around 125.5 GeV [1, 2] puts the
studies of the Higgs sector of the MSSM in an entirely new perspective. In order to
remain viable, a point in the MSSM parameter space must now not only pass all the
(ever stricter) experimental bounds on superparticle masses, but also lead to the
prediction of a scalar with mass, production cross section and decay rates compati-
ble with those measured at the LHC. In particular, the relatively large mass of the
roughly-SM-like scalar discovered at the LHC implies either very heavy stops, of the
order of 3 TeV, or a large value of the left-right stop mixing term (see, e.g., Refs.
[648,649]). The benchmark scenarios routinely considered in MSSM studies had
been devised when the Higgs sector was constrained only by the LEP searches, and
many of them, such as the so-called no-mixing scenario, are now ruled out because
they predict a too-light SM-like scalar. Others, such as the so-called mmax scenario,
are constrained for the opposite reason, i.e. they can predict a too-heavy SM-like
scalar. h To address the need for new benchmark scenarios to be used in future
studies of the MSSM Higgs sector, in Section 14.2 we will define scenarios that are
compatible both with the properties of the Higgs boson discovered at the LHC and
with the current bounds on superparticle masses. The fact that information on the
Higgs boson mass, production and decays has now become avail- able also puts new
emphasis on the need for accurate theoretical predictions of those quantities. In the
studies presented in this report, the masses and mixing of the MSSM Higgs bosons
are computed with the public code F EYN H IGGS [2427], which implements the
full one-loop radiative corrections together with the dominant two-loop effects. The
theoretical accuracy of the prediction of F EYN H IGGS for the

lightest-scalar mass was estimated to be of the order of 3 GeV [26, 650, 651],
i.e., already comparable to the accuracy of the mass measurement at the LHC.
Improving the accuracy of the theoretical predic- tion for the MSSM Higgs masses
will require the inclusion in public computer codes of the remaining two-loop effects
[652654] and at least the dominant three-loop effects [655657]. The production
and decay rates of a SM-like Higgs boson in the MSSM are sensitive to contri-
butions from virtual SUSY particles, and their measurement at the LHC combined
with the searches for additional Higgs bosons can be used to constrain the MSSM
parameter space. To this effect, the theoretical predictions for cross section and
decays must include precise computations of the SUSY con- tributions. In Section
14.3 we use the public code S US H I [641] and the POWHEG implementation
of Ref. [77] to compute the total and differential cross sections for neutral Higgs-
boson production in gluon fusion, including a NLO-QCD calculation of quark and
squark contributions plus higher-order quark contributions adapted from the SM
calculation. We show that the SUSY contributions can be sizeable in regions of
the MSSM parameter space where the third-generation squarks are relatively light,
and discuss the theoretical uncertainty of the predictions for the cross sections.
Finally, we study and update the exclusion limits on light charged MSSM Higgs
bosons in the (MH , tan)-plane in various benchmark scenarios in Section 14.4.
Particular emphasis is placed on the dependence of the limits on the variation of
SUSY parameters. We also provide improved NLO- QCD cross section predictions
for heavy charged Higgs production in the so-called four and five-flavor schemes in
Section 14.5. The five-flavor scheme cross section is calculated with a new scheme

for setting the factorization scale and takes into account the theoretical uncertainty from scale variation and the PDF, s and bottom-mass error. We observe good agreement between the 4FS and 5FS NLO-calculations and provide a combined prediction following the Santander matching. 14.2 New MSSM benchmark scenarios Within the MSSM an obvious possibility is to interpret the new state at about 125.5 GeV as the light CP-even Higgs boson [334, 338, 648, 649, 658662]. At the same time, the search for the other Higgs bosons has continued. The non-observation of any additional state in the other Higgs search channels puts by now stringent constraints on the MSSM parameter space, in particular on the values of the tree- level parameters MA (or MH) and tan . Similarly, the non-observation of supersymmetric (SUSY) particles puts relevant constraints on the masses of the first and second generation scalar quarks and the gluino, and to lesser degree on the stop and sbottom masses (see Refs. [663, 664] for a recent summary). Due to the large number of free parameters, a complete scan of the MSSM parameter space is impractical in experimental analyses and phenomenological studies. Therefore, the Higgs search results at LEP were interpreted [458] in several benchmark scenarios [16, 665]. In these scenarios only the two parameters that enter the Higgs sector tree-level predictions, MA and tan , are varied (and the results are usually displayed in the MA tan plane), whereas the other SUSY parameters, entering via radiative corrections, are fixed to particular benchmark values which are chosen to exhibit certain features of the MSSM Higgs phenomenology. These scenarios were also employed for the MSSM Higgs searches at the Tevatron and at the LHC. By now, most of the parameter space of the original benchmark scenarios [16, 665] has been ruled out by the requirement that one of the CP-even Higgs boson masses should be around 125.5 GeV. Consequently, new scenarios have been proposed [31], which are defined such that over large parts of their available parameter space the observed signal at about 125.5 GeV can be interpreted in terms of one of the (neutral) Higgs bosons, while the scenarios exhibit interesting phenomenology for the MSSM Higgs sector. The benchmark scenarios are all specified using low-energy MSSM parameters, i.e. no particular soft SUSY-breaking scenario was assumed. Constraints from direct searches for Higgs bosons are taken into account, whereas indirect constraints from requiring the correct cold dark matter density, BR(b s), BR(Bs +) or (g2) are neglected. However interesting, those constraints de

Chapter 2

The Search for neutral MSSM Higgs Bosons in the final state: $\tau^+\tau^- \rightarrow e\mu + 4\nu$

This chapter presents the search for the neutral MSSM Higgs bosons decaying in tau pairs and fully leptonic final state. This search is based on 20.3 fb^{-1} of 8 TeV data recorded by ATLAS experiment during 2012 at Large Hadron Collider (LHC) [1]. In this analysis two channels are employed by requiring the presence or absence of a b-tagged jet, this increases the sensitivity to the neutral MSSM Higgs boson via the b-associated and gluon-gluon fusion production modes, respectively. Data driven methods are used to estimate $Z \rightarrow \tau\tau$ an QCD multi-jet backgrounds.

The chapter is divided in four sections: in section 2.1 an introduction to experimental searches and to the strategy of this particular analysis is given, in section 2.2 the background model estimation is described, while in section 2.3 methods to evaluate systematics uncertaities are discussed, finally in section 2.4 the result of the sarch are presented.
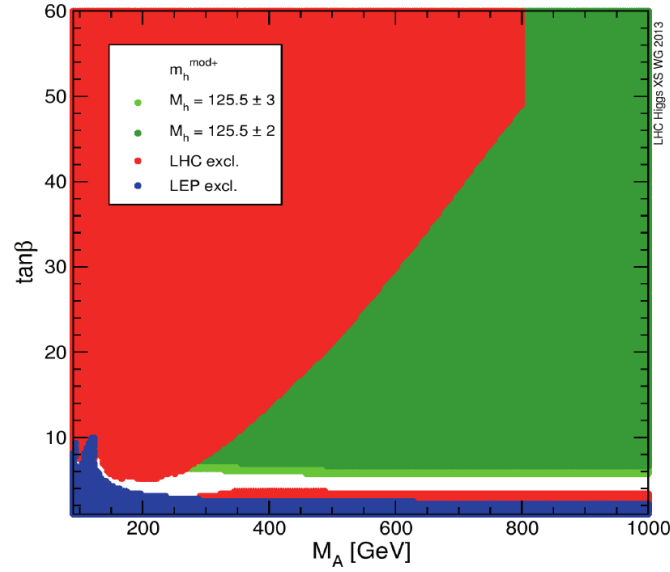
Figure 2.1: $m_A - \tan\beta$ plane for the m_h^{mod+} scenario, with excluded region from direct Higgs searches at Lep (blue) and LHC (red). The two green shades corresponds to the allowed parameter space for the assumption of $M_h = 125.5 \pm 2(3)$ GeV. For more detail see [].

2.1   The Search Strategy

2.1.1   Motivation

Under the light of the recent discovery of a Higgs boson with mass of 125 GeV [], remains an open question wheter this new particle constitute all the pieces of the Higgs sector or wheter it is only one of several bosons predicted in some theories that go beyond the SM. The most recent measurements [] of its properties shows it to be, within experimental uncertainties, perfectly compatible with the SM Higgs boson, however such a new particle can be accomodated within several beyond the standard model (BSM) theories, this is particularly true for Super Symmetry.

There are two approach to explore the Higgs sector: one can study the cupling of the Higgs boson with vector bosons and fermions, those measure in fact are sensitive to new physics and can determine if this particle is fully responsible for the generation of all the SM particles masses. Another approach is to directly search for for additional Higgses in a well defined model, which is the approach followed in this thesis where new neutral bosons are sought within the MSSM (see chapter **??**).

In the MSSM a Higgs boson with properties that resembles the one for a SM Higgs boson occures naturally in large regions of parameter space, for practical reason however, is usefull to fix parameter of the model to achieve what is called a benchmark scenario. With the recent discovery, bechmark scenarios of the MSSM have been updated to fit with the new constraints (more details on benchmark scenarios are in chapter **??**), as an example in figure **??** are reported the current

exclusion limits for one of those updated scenarios, m_h^{mod+}, the green area represents what is currently allowed in the $m_A - \tan\beta$ plane showing that there is still plenty of room for BSM Higges.

2.1.2 How to search for new phenomena?

In experimental physiscs an observation of a new phenomena or its exclusion is carachterized by means of statistical statements, in this sense one can say that statistic is the language of experimental physics. Search for new physics at the LHC extesively uses frequentistic statistical tests [**?**]. In this section an itroduction to statistical tests is given, for more details see section **??**.

A *statistical test* is a rule to reject or accept an hypotesis, where for hypotesis is meant a statement about the distribution of the data. Typically new physics searches are looking for a signal that is additive on top of the background, is then natural to compare two hypotesis: the background only hypotesis H_0, or null hypotesis, and the signal plus background hypotesis H_1, which is the alternative. In the process of decision making is common to define what is called a *signal region* (SR), which is simply a set of selections applied to data aimed to enhance signal with respect to the background, the observed number of events in the SR, N_{SR}, are used to make probabilistic statements about the two hypotesis. N_{SR} is in fact a random variable described by a Poisson distribution where, in case the null hypotesis is true, ν_B events are expected, otherwise in case H_1 is true $\nu_B + \nu_S$ events are expected. The two probability distributions for the two hypotesis totaly describes the *probability model* for this counting experiment. Is clear then that the evidence for a signal shows up as an excess of events, a way to quantify the conpatibility of the null hypotesis with data is to make a *significance* test: calculate the probability that the background-only would produce at least as many as the observed events, which is the so called of p-value and in this case is expressed by the formula:

$$\text{p-value} = \sum_{n=N_{SR}}^{\infty} \text{Pois}(n|\nu_B)$$

Calculating p-values is a way to characterize an excess, in high energy physics the commonly accepted p-value that is qualified as a discovery is 2.87×10^{-7}, which is an extremely low probability for the null hypotesis to be true and corresponds to five standard deviation for a gaussian distribution.

In case no excess is observed, the procedure is to build a statisctical test where the null hypotesis is accepted and at the same time the signal hypotesis is rejected with a fixed predetermined probability, called confidence level. A statistical test is a rule that defines a region in the space of data for which a given hypotesis can be accepted or rejected, often rather than using a full set of data $\mathcal{D}$, it is convenient to define a *test statistic*, T, which is usually a single number computed from the data, the two hypotesis implies different distributions for T, then one defines an acceptance region W in terms of the test statistic, if $T \in W$ the H_0 is rejected, H_1 accepted and vice versa, the probability with which one rejects H_1 or H_0 is then given by the choice of W and T. Neuman and Pearson provided a framework for hypotesis testing that addresses the choice of the test statistic [**?**].

A discriminating variable is often used to help separating signal and backgrounds, this can be any of the observables of the experiment, a usually chosen observable is for example the invariant mass of the final state particles. The expected distributions of this observable for the two hypotesis completes the above mentioned probability model, the actual implementation is achieved by means of an histograms, i.e. by discretizing the distribution of the observable and making a counting experiment for each bin of the histogram, the resulting probability model is then a product of Poissons:

$$\prod_i \mathrm{Pois}(n_i^{observed} \mid s_i(\vec{\theta}) + b_i(\vec{\theta})) \tag{2.1}$$

where s_i and b_i are the number of expected signal and background events in the bin i, while n_i are the actual observed events in the bin i. Here is made explicit that the signal and backgrounds expectations depends also on a set of additional parameter $\vec{\theta}$, called *nuissance parameters*, those embed effects like detector mismodeling and theoretical uncertainty.

Summarizing, there are several ingredients that constitute a search for new physics:

- Definition of a signal region in data where signal is enhanced with respect to the backgrounds, detailed for this analysis in section **??** and **??**.

- Definition of a discriminating variable which is usefull to disentangle between signal and backgrounds, see section **??**.

- Definition of the probability model, i.e., the expectation for the distribution of the discriminating variable for signal and background hypotesis, this is one of the most importat point of a search and main part of the work of this thesis, detailed in section **??**.

- Definition of a test statistics to quantify an observation or an exclusion, which is discussed for the LHC in section **??**.

2.1.3 Signal Topology

This section describes the strategy to enhance the search sensitivity taking advantage of the signal topology. The Sensitivity of a search is the signal strenght that is expected to be excluded in case of no signal. If one is searching for a rare process, then the analysis strategy, i.e. the plan or the steps to enhance the signal sensitivity of the search, is crucial. This search is complementary to the Standard Model Higgs search in tau final state, this is also considered in the analysis strategy, the focus is then on phase space not explored from SM search.

In the MSSM for large region of parameter space one found that one of the CP-even neutral Higgses has properties that resemble the one of the SM Higgs, this is usually the case for the lightest Higgs, h, the other two, H and A, tend to be degenerate in mass and decouple from gauge bosons. An interesting fenomenological consequence is that the coupling of the latter two Higgses with down (up) type
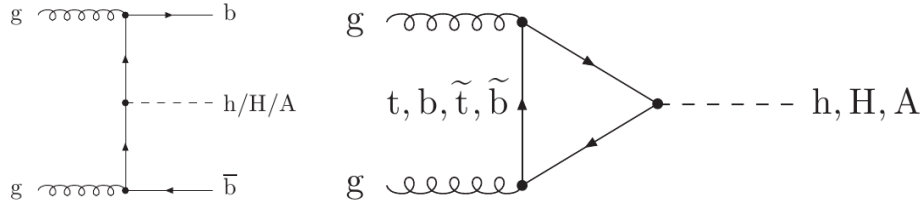
Figure 2.2: Feynman diagram for b-associated production and gluon-gluon fusion for MSSM neutral Higgs.

fermions are enhanced (suppressed) by $\tan\beta$, meaning that for large $\tan\beta$ bottom-quark and τ lepton will play a more important role than in the SM case either for production and decay.

The production of the neutral CP-even MSSM Higgs bosons at hadron colliders proceeds via the same processes as for the SM Higgs production. However, the pseudoscalar A instead cannot be produced in association with gauge bosons or in vector boson fusion (VBF) at tree-level, as this coupling is forbidden due to CP-invariance. At the LHC one of the most relevant production mechanisms for the MSSM Higgs bosons is gluon-gluon fusion, $gg \to A/H/h$. In addition, the production in association with b-quarks becomes important for large value of $\tan\beta$. Those are the two production mechanism that are considered in this analysis, figure 2.2 shows the feyinman-diagram for those processes, while figure 2.3 shows the production cross section of the neutral MSSM Higgses via these two processes. The search is divided in two category which are optimized for the two different production mode considered, in the gluon-fusion category is requred a b-jet veto (for definition of b-tagging algorithm see chapter **??**), in fact no b-jet in the final state are present for this production mode. In contrast a a b-jet tag is required for b-associated production, this category is expected to be very sensitive to $\tan\beta$. The two category are ortogonal and present different backgrounds contributions, which can be optimized separately.

The decays of the neutral MSSM Higgs bosons (in the assumption that all supersymmetric particle are heavy enough) are the same as for the SM one with the already cited exception of A. Figure 2.3 shows the decay branching fractions for H and A as a function of the mass, the decay into tau pair is the most important after $b\bar{b}$ and the one used in this analysis. The decay channel in $b\bar{b}$ is in fact very challenging due to the huge background from QCD multi-jet. In this thesis only cases in which the taus decay one in $e + 2\nu$ and the other in $\mu + 2\nu$ are considered, This final state corresponds to a total $\tau^{+}\tau^{-}$ branching ratio of approximately 6%.

Summarising, the signal topology is characterised by a final state with an electron, a muon, and missing transverse energy due to the presence of four neutrinos from the τ decays. Furthermore, the final state may be split by the presence or absence of a b-quark initiated jet, depending on the production process. This signature is achieved experimentally by requiring:

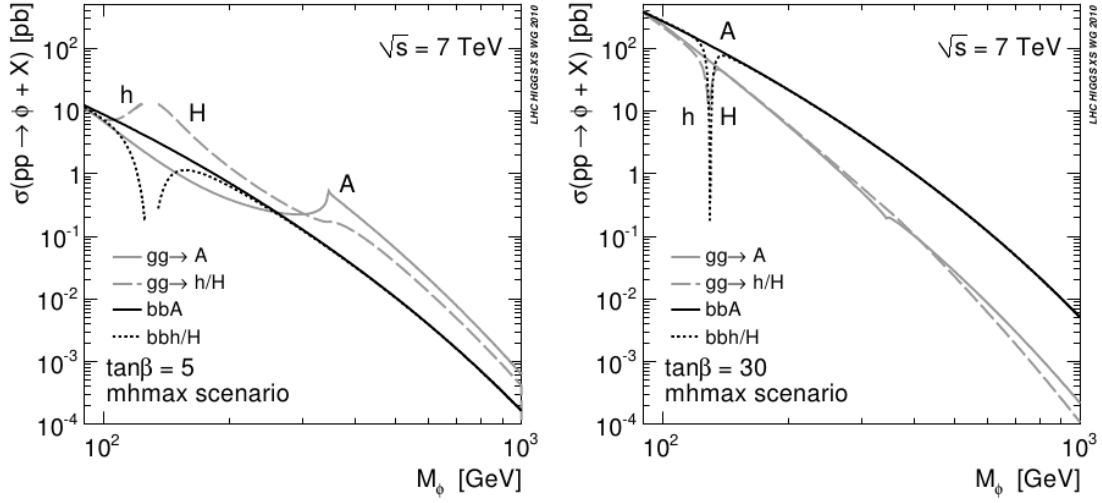(i) An OR between an elecron and an electron-muon trigger (`EF_e24vhi_medium1 || EF_e12Tvh_medium1_mu8`).

Figure 2.3: Production cross section for the $h/H/A$ MSSM neutral Higgs bosons via b-associated production and gluon-gluon fusion production mode. The calculation are for the m_h^{max} scenario and for $\tan\beta = 5$ (left) and $\tan\beta = 30$ (right).

(ii) Exactly one reconstructed electron and one muon of opposite charge, the muon is required to have $p_t > 10$ GeV, while the electron should have $p_t > 15$ or 25 GeV depending on the trigger that selected the event. For electron and muon object definition see chapter **??**.

(iii) The two leptons should be isolated, meaning that in a cone around the lepton there should be little energy deposit (should not be sorraunded by other particle, common of non-promt leptons coming from jets). For more detail about isolation properties see section **??**.

(iv) Hadronic τ veto: the events is rejected if at least one hadronic τ is found with $p_t > 15$ GeV.

(v) Lepton invariant mass greather than 30 GeV.

This set of selection all togheter are referred in the following as *preselection*. Full detail on preselections regarding all the quality requirements on object reconstruction are reported in appendix **??**. The two analysis category, *b-tag* and *b-veto*, are defined adding on top of the preselections the request of "exactly one b-tagged jet" or "no b-tagged jet" in the event respectively, to be *taggable* a jet should have $p_t > 20$ GeV and $|\eta| < 2.5$ (for full definitions of b-tagging and jets see chapter **??**).

2.1.4   How to deal with Backgrounds

The signal topology described in the previous section is common to many other processes, unfortunately, those have higher cross section than the sought signal and a set of additional selections is needed to enhance the sensitivity of the search. The most important backgrounds to this search are the production of $Z \rightarrow \tau\tau$ + jets, the
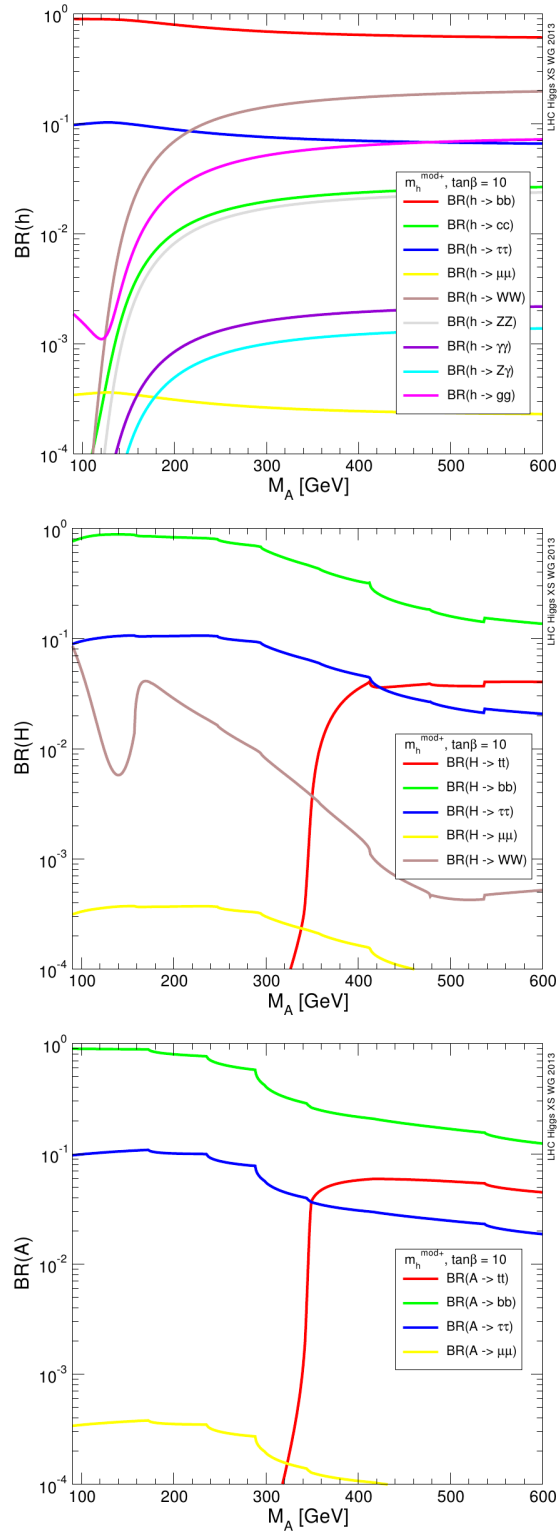
Figure 2.4: Branching fraction for the MSSM neutral higgses $h/H/A$ in the m_h^{mod+} scenario.

top quark ($t\bar{t}$ and single top production is intended), diboson production (like WW or ZZ events) and Drell-Yan process or events with non-prompt leptons coming solely from hadron decay (in short QCD multi-jet). Vector bosons production like $W \to \ell\nu$ or $Z \to \ell\ell +$ jets (with ℓ here meaning either e or μ) are also considered, however those processes have a limited impact.

The final state of Higgs decaying into tau pair coincide with the one from $Z \to \tau\tau$ process, this is then an irreducible background. Exploiting the different kinematics of the Higgs decay with respect to other backgrounds it possible to disentangle between the two. In the Higgs decaying into $\tau^+\tau^- \to e\ \mu + 4\nu$ the taus are highly boosted and this feature is transferred to the final state leptons, their kinematics then result to be significantly different with respect to process like diboson or $t\bar{t}$. A first difference is that e and μ from the Higgs decay will be more likely "back-to-back", as it is shown in Figure 2.5(a) where the angle between the leptons in the transverse plane $\Delta\phi = |\phi_e - \phi_\mu|$ is reported. Furthermore the neutrinos will be more likely collinear with the charged leptons: this feature can be matematically seen as the sum of scalar product between missing energy and the leptons four-vectors in the transverse plane, if the vectors are normalised to unit versors then what remains is a relation only between angles:

$$\hat{E}_T^{miss} \cdot (\hat{P}_T^\mu + \hat{P}_T^e) = cos(\Delta\phi_{E_T,\mu}) + cos(\Delta\phi_{E_T,e}) = \sum_\ell cos(\Delta\phi_{E_T,\ell})$$

collinearity implies this sum to be equal to zero as it is shown in figure 2.5(b). These two feature can be used to distinguish between mu-e coming from decay from highly boosted object and the one coming from W decays in top or in dibosons backgrounds which will have a more spread distribution. In b-veto category these two variables are sufficient to suppress contribution from dibosons, no other selection is applied in this category because it has been shown to not bring significant improvement.

In the b-tag category the situation is different, the request of b-jet enhance backgrounds with high jet activity as top production, given the relatively low jet activity of Higgs events (also in the case of b-associated production) it is possible to separate them from top production which instead is very likely to have two or more highly enegetic jets in the event. Little jet activity is achieved by requesting requesting the sum of the jets p_t in the event to be small, this variable is called H_T and is shown in figure 2.5(c). Another feature that distinguish top pair production from Higgs is the much higher invariant mass of the former final state, in the transverse plane all the leptons will tend to have a higher momentum, the sum of lepton p_t and E_T^{miss} is then used as a discriminating variable. Figure 2.5(d) shows the distribution of this last analysis variable.

The above described variables defines the signal region in the b-tag and b-veto category, in table 2.1 a summary of the preselection and all the selection variable used with their optimized cut values is reported. Figure 2.6 shows the final state invariant mass distribution (here the MMC_{mass} discriminating variable is used see section 2.1.5) as a function of the selection stage, while in tables 2.3-2.2 the number of events that survises at each cut stage for different background is reported.
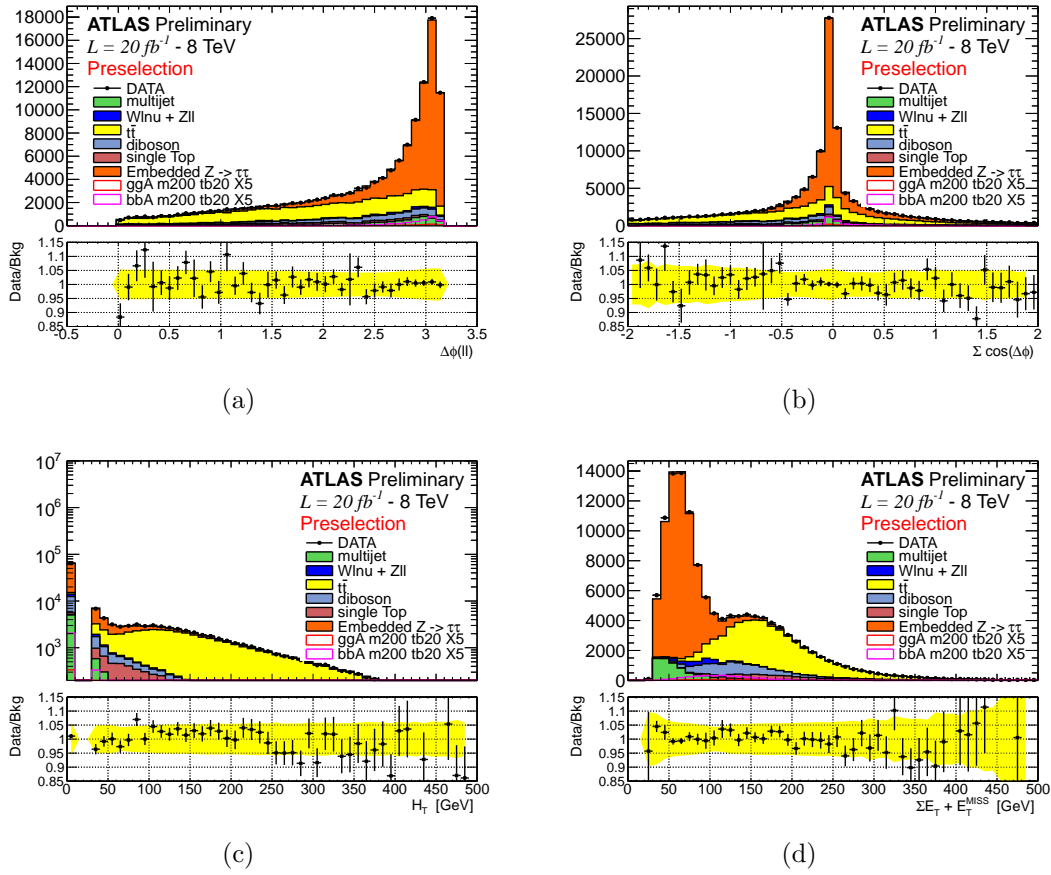
Figure 2.5: Distribution of analysis variable after preselection.

2.1.5   Mass Reconstruction with MMC Technique

Reconstructing the invariant mass of a di-tau system from the tau decay products is a challenging task due to the presence of neutrinos in the final state. In a di-tau system in which both taus decays leptonically (with a total of four neutrinos) there are eight uknowns, those are the components of the two four-vectors that represents the missing momentum (carried out by neutrinos) in each tau decay. There are four additional constraint which come from the measures of E_T^{miss} and from the fact that each single decay should have invariant mass equal to the tau mass, therefore there are still four degrees of freedom in the system. Several approximation are possible to further constraint the momentum carried by neutrinos, for example assuming them collinear to the other leptons from tau decay, however those approximation suffers of limitations.

In this analysis, the so-called "Missing Mass Calculator" (MMC) [55] is used to calculate the di-tau system invariant mass from its decay products and the E_T^{miss}. This technique employs additional information from the well known tau decay to constraint the system: in the above mentioned four dimensional parameter space, in which lies the solution of the di-tau system, not all the points are equally likely for a given event topology, using Pythia simulation supplemented with TAUOLA package, a likelihood based on $\Delta R = \sqrt{\Delta\eta^2 + \Delta\phi^2}$ distribution between the missing energy and each of the two "visible" leptons is build, minimising the likelihood for a given event topology it is possible to determine the most likely point in the parameter space and solve the system. Effect of resolution are taken into account by producing a mass distribution for each of the scanned points in the parameter space. As a result this method give a more precise measurement of the di-tau system invariant mass and a considerable improvement in resolution. The invariant mass distribution calculated with the MMC technique is referred in the following as MMC_{mass} and is used as discriminating variable in the limits setting.

2.2   Background Modeling and Validation

This section describes the strategies for background modeling and validation. Monte Carlo (MC) simulation is extesively used for model either background and signal, in section 2.2.1 a brief description of the simulated sample used is given.

Monte Carlo simulations of any process are usually prone to systematics uncertainties due to non-perfect descriptions of pileup effects, underlying event and detector performance, therefore, data-driven background esimation method are employed for the estimate of $Z \to \tau\tau$ and QCD multijet backgrounds, described respectively in section 2.2.4 and 2.2.3. Other background processes, such as $t\bar{t}$, single top, dibosons, $Z \to ll + $ jets (where $l = e, \mu$) and W + jets, are estimated using MC predictions. Given the particular importance of $t\bar{t}$ a dedicated study to validate this background has been made and described in section 2.2.2.
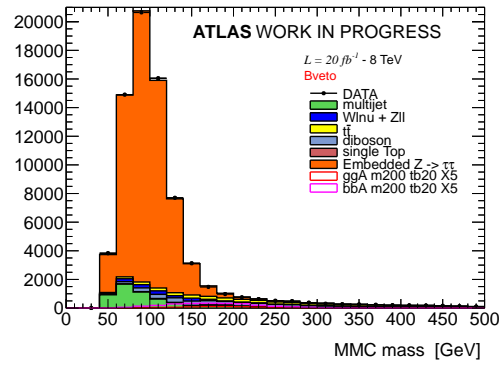
In this section we make use of analysis tools, quality requirements and object definition (like electrons, jet and muon) described in chapter **??**. Furthermore a set corrections is applied to simulated events to take into the non perfect description of detector performance and response, full detail on those corrections is reported
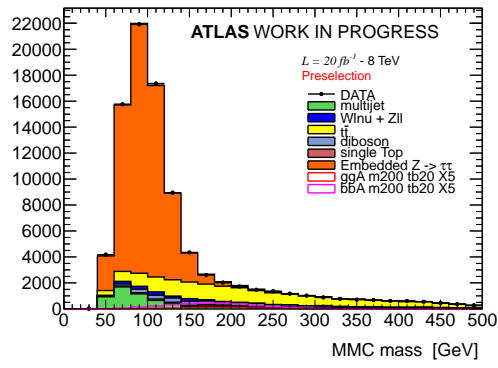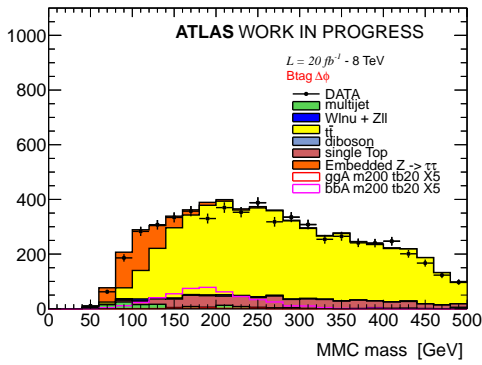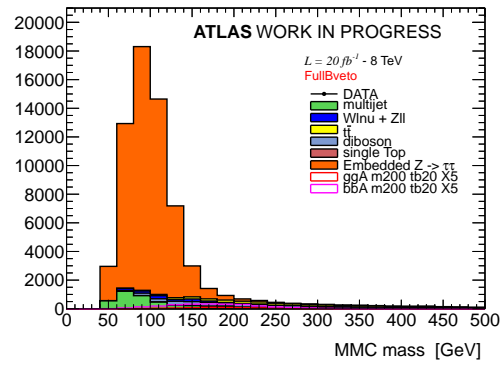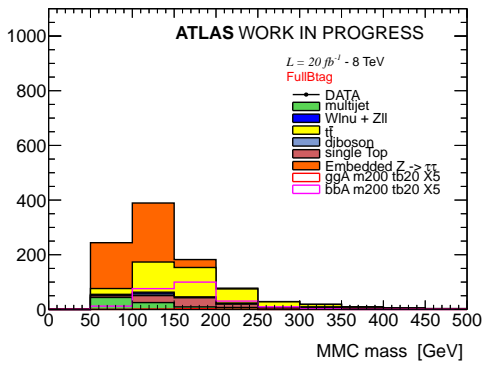
(a)
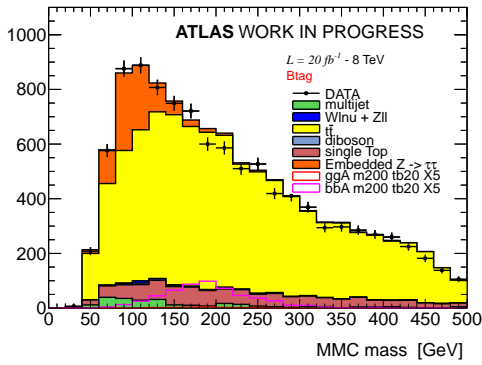
(b)

(c)

(d)

(e)

(f)

Figure 2.6: Distribution of the MMC_{mass} for different cuts stage, see text. Left column corresponds to b-tag category, right column to b-veto.

Channel	Selection
Preselection	Trigger
	At least one reconstructed vertex
	Event cleaning
	Tau Veto
	Exactly one tight isolated electron with $p_t > 15$ or 25 GeV (trigger dependent)
	Exactly one Combined isolated muon with $p_t > 10$ GeV
	Opposite charge between the leptons
b-Tag	Exactly one b-tagged taggable jet
	$\Delta\phi(e-\mu) > 2$
	$\sum \cos\Delta\phi > -0.2$
	$\sum H_T < 100$ GeV
	$\sum L_T + E_T^{miss} < 100$ GeV
	Good MMC solution
b-Veto	Exactly zero b-tagged taggable jets
	$\Delta\phi(e-\mu) > 1.6$
	$\sum \cos\Delta\phi > -0.4$
	Good MMC solution

Table 2.1: Summary of the preselection and the full selections used for the b-tag and b-veto channels.

in appendix **??**. Systematic uncertainties on the background model predictions are detailed in Section 2.3.

A good agreement between data and background model is found after preselections, this is supported by figure 2.7 which shows few kinematic variables and figure 2.5 which shows analysis selection variables after preselection.

2.2.1   Simulated Event Samples

Signal production via the gluon fusion process, $gg \rightarrow A/H/h$, was simulated with POWHEG [30] and the associated $b\bar{b}A/H/h$ production with SHERPA [31]. The pseudoscalar Higgs boson samples were generated in the mass range from 90 GeV to 300 GeV and at $\tan\beta = 20$, the same kinematics are assumed for $A/h/H$ Higgs bosons decay products and at other $\tan\beta$ values, appropriate reweighting is applied according to the different cross-sections. The $m_h^{\max}$ MSSM benchmark scenario [34] is assumed.

The production of W and Z/γ^* bosons in association with jets was simulated with the ALPGEN [23] generator. The $t\bar{t}$ process was generated using the POWHEG generator. The single-top (s-channel, Wt) processes were generated using MC@NLO [25], while single-top (t-channel) processes were generated with AcerMC [26]. The production of diboson (WW, WZ, ZZ) were generated with HERWIG [27]. For all ALPGEN and MC@NLO samples described above, the parton shower and hadronisation were simulated with HERWIG and the activity of the underlying event with JIMMY [28]. Different parton density functions (PDFs) sets are used depending on the generator - CTEQ6L1 [32] is used by ALPGEN and AcerMC while CT10 [33] is used by SHERPA, POWHEG and MC@NLO.

TAUOLA [36] and PHOTOS [37] are used to model the tau lepton decay and

	Preselection	n(b-jet)=1	$\Delta\phi(e-\mu) > 2$	$\sum \cos\Delta\phi > -0.2$	$\sum L_T + E_T^{miss} < 100$ GeV	$\sum H_T < 100$ GeV	mmc
Data	125886	23352	-	-	-	-	-
Multijet	6700 ± 500	330 ± 40	208 ± 27	135 ± 22	114 ± 17	100 ± 15	100 ± 15
$Z \to \ell\ell$	570 ± 50	5.2 ± 1.8	2.3 ± 1.1	2.3 ± 1.1	1.7 ± 1.0	0.9 ± 0.8	0.9 ± 0.8
$W \to \ell\nu$	1630 ± 150	20 ± 6	15 ± 6	13 ± 6	10 ± 6	10 ± 6	10 ± 6
Diboson	9340 ± 50	99 ± 5	63 ± 4	36.4 ± 3.0	14.8 ± 1.8	13.3 ± 1.8	13.1 ± 1.8
$t\bar{t}$	40630 ± 110	19810 ± 70	9680 ± 50	6450 ± 50	808 ± 15	350 ± 10	330 ± 10
Single Top	4450 ± 40	2456 ± 33	1223 ± 23	784 ± 18	122 ± 7	99 ± 7	90 ± 6
$Z \to \tau\tau$	61500 ± 70	952 ± 9	625 ± 7	540 ± 7	482 ± 6	421 ± 6	418 ± 6
Signal	-	-	-	-	-	-	-

Table 2.2: Number of data and background events in the b-tag channel.

	Preselection	n(b-jet)=0	$\Delta\phi(e-\mu) > 1.6$	$\sum \cos \Delta\phi > -0.4$	mmc
Data	125886	89155	-	-	-
Multijet	6693 ± 456	6357 ± 461	5322 ± 438	4137 ± 339	3934 ± 335
$Z \to \ell\ell$	569 ± 48	564 ± 48	516 ± 47	434 ± 44	432 ± 44
$W \to \ell\nu$	1625 ± 155	1604 ± 155	1145 ± 125	714 ± 101	656 ± 100
Diboson	9338 ± 48	9235 ± 48	7358 ± 43	4002 ± 31	2925 ± 27
$t\bar{t}$	40632 ± 106	7707 ± 46	5044 ± 37	3416 ± 31	2159 ± 24
Single Top	4449 ± 44	1664 ± 27	1124 ± 22	682 ± 18	435 ± 14
$Z \to \tau\tau$	61503 ± 68	60440 ± 67	58078 ± 65	55303 ± 64	54683 ± 63
Signal			-	-	-

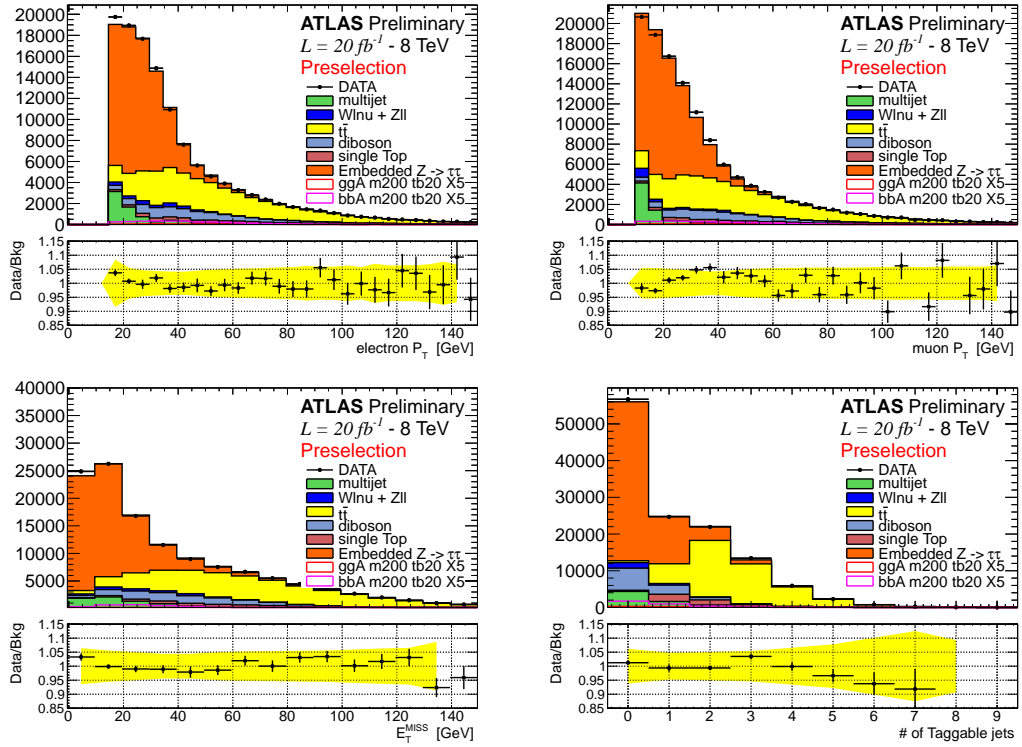Table 2.3: Number of data and background events in the b-veto channel.

Figure 2.7: Distribution of some kinematic variables after preselection.

Process	Cross-section (pb) [× BR]
$W \to \ell$+jets ($\ell = e, \mu, \tau$)	12.22×10^3
$Z/\gamma^* \to \ell\ell$+jets ($m_{\ell\ell} > 60$ GeV)	1.15×10^3
$Z/\gamma^* \to \ell\ell$+jets ($10 < m_{\ell\ell} < 60$ GeV)	4.35×10^3
$t\bar{t}$	137.3
Single top t-, s- and Wt-channels	28.4, 1.8, 22.4
Diboson WW, WZ and ZZ	20.6, 6.8, 1.55
Signal ($m_A = 150$ GeV, $\tan\beta = 20$, m_h^{max} scenario)	
$gg \to A \times \mathrm{BR}(A \to \tau\tau) \times \mathrm{BR}(\tau\tau \to e\mu + 4\nu)$	$16.8 \times 0.118 \times 0.062$
$gg \to H \times \mathrm{BR}(H \to \tau\tau) \times \mathrm{BR}(\tau\tau \to e\mu + 4\nu)$ ($m_H = 151$ GeV)	$18.4 \times 0.119 \times 0.062$
$gg \to h \times \mathrm{BR}(h \to \tau\tau) \times \mathrm{BR}(\tau\tau \to e\mu + 4\nu)$ ($m_h = 129$ GeV)	$13.7 \times 0.110 \times 0.062$
$b\bar{b}A \times \mathrm{BR}(A \to \tau\tau) \times \mathrm{BR}(\tau\tau \to e\mu + 4\nu)$	$39.4 \times 0.118 \times 0.062$
$b\bar{b}H \times \mathrm{BR}(H \to \tau\tau) \times \mathrm{BR}(\tau\tau \to e\mu + 4\nu)$ ($m_H = 151$ GeV)	$35.7 \times 0.119 \times 0.062$
$b\bar{b}h \times \mathrm{BR}(h \to \tau\tau) \times \mathrm{BR}(\tau\tau \to e\mu + 4\nu)$ ($m_h = 129$ GeV)	$4.71 \times 0.110 \times 0.062$

Table 2.4: The cross sections (multiplied by the relevant branching ratios (BR)) used in this note. Signal cross sections are shown for $m_A = 150$ GeV and $\tan\beta = 20$

additional photon radiation from charged leptons in the leading-log approximation, respectively, except for SHERPA samples.

All MC event samples were passed through the full simulation of the ATLAS detector using GEANT4 [38, 39] The effects of the simultaneous recording of several events from the same or neighbouring bunch crossings (pile-up) are considered in the simulation.

The cross-sections of the MC event samples used in this note are summarised in Table 2.4. The W/Z+jets and $b\bar{b}A/H/h \to \tau\tau$ cross sections are calculated to NNLO. Those for $t\bar{t}$ comes from direct cross section measurement []. The single top and diboson cross sections are calculated at NLO for single top and dibosons. Finally, the direct $gg \to A/H/h \to \tau\tau$ signal cross sections are calculated at NNLO and NLO for the top loop and the bottom loop and top/bottom loops interference, respectively.

2.2.2 Top Quark Pair Production Validation

The background from top quark pair production is estimated using a sample of events from the POWHEG-PYTHIA MC generator. Since this is one of the major backgrounds for this analysis a careful validation is needed, for this purpose a $t\bar{t}$ rich control region is defined using events passing the preselection with the additional requirement of two b-tagged jets. Figures 2.8 and 2.9 show a set of kinematic and analysis selection variables in this CR, for both data and the MC prediction, good agreement between data and the background model is found: an overall data to background ratio of 0.998 ± 0.011(stat.) ± 0.110(sys.) is observed. The total systematic uncertainty on the ratio is dominated by the uncertainty on the b-tagging efficiency.
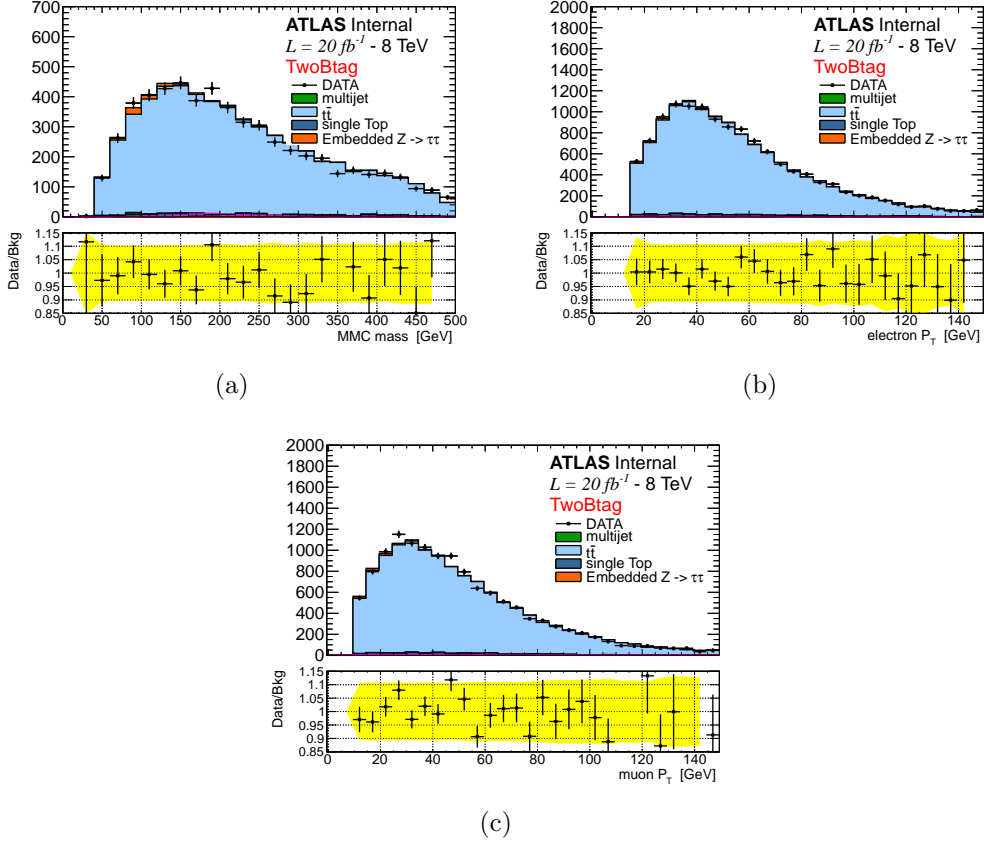
(a)

(b)

(c)

Figure 2.8: Distributions of a) the MMC mass, b) the transverse momentum of the electron $p_t(e)$ and c) the transverse momentum of the muon $p_t(\mu)$, for both data and MC in the $t\bar{t}$ control region. The uncertainties on the points for the ratio plot show the statistical uncertainty on the data to background ratio, whereas the yellow band show the total systematic uncertainty on this ratio.

Figure 2.9: Distributions of a) $\Delta\phi(e - \mu)$, b) $\sum \cos \Delta\phi$, c) $\sum L_T + E_T^{miss}$ and d) H_T, for both data and MC in the $t\bar{t}$ control region. The uncertainty on the points for the ratio plot show the statistical uncertainty on the data to background ratio, whereas the yellow band show the total systematic uncertainty on this ratio.
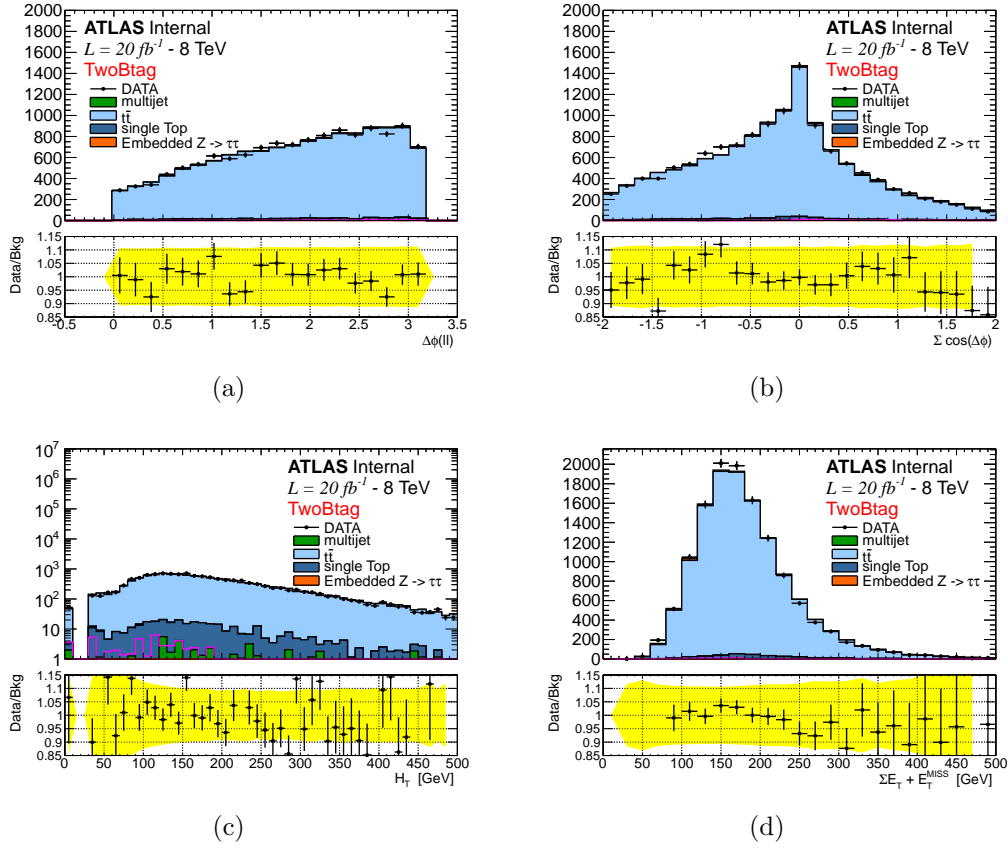
2.2.3 Multi-jet Background

The QCD multi-jet background represents an important background, especially in the b-veto category, due to its high cross-section and the relatively low cut on lepton p_t used in this analysis. This background is evaluated by a data-driven technique, the so-called ABCD method. The ABCD method consists of splitting the data sample in four regions: the signal region (SR) and three control regions (CR), where the control regions are mutually orthogonal and designed to be enriched in multi-jets events. The four regions are defined by using the charge correlation between the leptons and isolation selections. With isolation is intended the sum of the energy deposit in a cone of fixed size around the lepton, this variable can be defined using calorimetric energy deposition or track momentum measurement done by the inner detector. To obtain regions rich in multi-jet background, the selections on both the calorimetric and tracking isolation are inverted with respect to the nominal ones defining anti-isolated leptons, is then possible to define four regions: opposite sign (OS) or same sign (SS) with respectively isolated or anti-isolated leptons. Historically the letters A-D are assigned to this regions for a

Region	Lepton Charge	Lepton Isolation
A (signal region)	OS	isolated
B	SS	isolated
C	OS	anti-isolated
D	SS	anti-isolated

Table 2.5: QCD background estimation control regions, defined by having leptons with opposite signs (OS) or same signs (SS) and by having the leptons either isolated or anti-isolated.

quicker reference as defined in Table 2.5.

An assumption of the ABCD method is that multi-jet backgrounds populate the OS and SS events independently of lepton isolation criteria, or in other words that the ratio of OS/SS events is uncorrelated with the lepton isolation selections. In this case, the number of QCD events in the signal region A can be estimated from the yield of multijet events in the control regions B, C and D, using the equation

$$N_A = N_B \times \frac{N_C}{N_D} = N_B \times R_{QCD} \tag{2.2}$$

To obtain the multijet yields in the data CRs, the contamination from electroweak (W+jets, Z+jets and dibosons) and top processes ($t\bar{t}$ and single top production) are subtracted in each control region using the MC prediction for their event yield. Tables 2.6 and 2.7 show the event yield for each CR throughout the full cut-flows along with the predictions of non-QCD multi-jets events which are subtracted. Signal contamination has been checked in all the three control regions for different mass points. For the range of m_A and $\tan\beta$ considered in this analysis, the highest signal contamination is seen in region B for the mass point $m_A = 300$ GeV and $\tan\beta = 50$, where a contamination of 0.2% is observed[1].

Shapes of kinematic distributions for QCD events are taken from region B, this region is expected to have similar kinematic property to the SR, however, suffers of either lower statistics and higher contamination with respect to region C or D. This choice is made to avoid a shape bias due to isolation requirements at trigger level (only the single-electron trigger ask for isolation), figure 2.10 shows the comparison between the electron p_t distributions in region B and D, in the latter high p_t electrons are suppressed, they do not pass trigger selections. Eventually the trigger isolation requirement could bias also the ratio OS/SS, this possibility has been checked carefully in a dedicated study and reported in Appendix A: to a good approximation, such trigger effects cancel out in the ratio OS/SS and no additional systematic is needed.

To test the ABCD method predictions an additional control region has been defined with the following selections:

- $E_T^{miss} < 20$ GeV

- $H_T < 70$ GeV and $\sum L_T + E_T^{miss} < 50$ GeV

---

[1] This value is mainly due to b-associated production and, as it scales with the cross section, for $\tan\beta = 20$ would be an order of magnitude smaller.
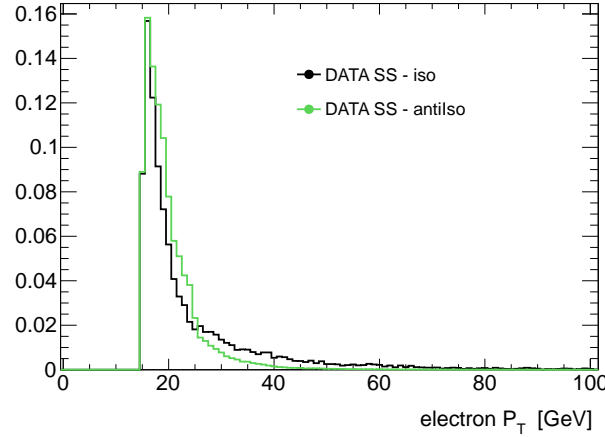
Figure 2.10: Comparison of the electron p_t distribution in region B and region D, showing the bias due to the trigger. The histograms are normalised to the same area.

- $0 < MMC_{mass} < 80$ GeV

This control region is designed to enhance multi-jet background with respect to $Z \to \tau\tau$ keeping the final state kinematics as similar as possible to the SR. Figure 2.11 shows the MMC_{mass} distribution for this CR with and without b-tagging requirements, agreement between data and the background model is found within statistical and detector related systematics uncertainty.

Systematic uncertainties are assigned on the scaling factor R_{QCD} and on the shape of the discriminating variable MMC_{mass} to take into account any correlation between isolation and charge of the leptons, details on the systematic uncertainty evaluation are addressed in Section 2.3.

2.2.4 $Z \to \tau\tau +$ Jets Background: Embedding Technique

The background from $Z \to \tau\tau$ decays is the major background to this analysis, a good uderstanding of it is then crucial. Unfortunately, for a light Higgs boson, it is impossible to completely separate $Z \to \tau\tau$ decays from the signal and a signal free data control region cannot be defined. However, thanks to the small Higgs coupling to muons, $Z \to \mu\mu$ decays provide a good starting point to model $Z \to \tau\tau$ events in a data-driven way. An hybrid Data-MC sample, known as "Embedding" is used to model the $Z \to \tau\tau$ background: $Z \to \mu\mu$ candidates are selected in data, then, the two muons from the Z decay are substituted with the decay products from simulated taus, this means that the energy deposit and tracks in a cone around the muon are subtracted and substituted with the one from τ decay, those taus have the same kinematics as the original muons. Further details on this technique may be found in [40, 41].

Trigger is not simulated in the embedding samples, the event yield is normalised to ALPGEN $Z \to \tau\tau$ at preselection stage. Furthermore a set of corrections, as described in [42], are applied to unfold from the original $Z \to \mu\mu$ trigger and

| Selection		B	C	D	R_{QCD}
Preselection	Data	6189	604628	312901	1.929 ± 0.004
	non-QCD	2510 ± 180	1090 ± 30	730 ± 35	
B-tag	Data	419	44619	27257	1.64 ± 0.01
	non-QCD	215 ± 10	310 ± 12	277 ± 13	
$\Delta\phi(e-\mu)$	Data	230	38810	23316	1.67 ± 0.01
	non-QCD	104 ± 6	200 ± 10	175 ± 7	
$\sum \cos \Delta\phi$	Data	149	31379	18779	1.67 ± 0.02
	non-QCD	67 ± 5	127 ± 8	114 ± 6	
$\sum H_T$	Data	83	27781	15626	1.78 ± 0.02
	non-QCD	23 ± 4	25 ± 3	22 ± 3	
$\sum L_T + E_T^{miss}$	Data	71	27735	15590	1.78 ± 0.02
	non-QCD	10 ± 3	22 ± 3	18 ± 2	
$MMC_{mass} > 0.$	Data	70	27634	15522	1.78 ± 0.02
	non-QCD	9 ± 3	20 ± 3	17 ± 2	

Table 2.6: QCD background estimation as a function of the analysis selections for the b-tagged category. The yields for the different control regions, as well as the scaling factor R_{QCD}, are reported. The error on the R_{QCD} is statistical only.

Selection		B	C	D	R_{QCD}
Preselection	Data	6189	604628	312901	1.929 ± 0.004
	non-QCD	2510 ± 180	1090 ± 30	730 ± 35	
B-veto	Data	5673	558217	284847	1.960 ± 0.004
	non-QCD	2220 ± 180	710 ± 30	415 ± 30	
$\Delta\phi(e-\mu)i$	Data	4610	532583	271404	1.962 ± 0.005
	non-QCD	1700 ± 170	580 ± 30	345 ± 30	
$\sum \cos \Delta\phi$	Data	3417	486747	247712	1.965 ± 0.005
	non-QCD	1120 ± 100	370 ± 20	230 ± 20	
$MMC_{mass} > 0.$	Data	3177	479967	244276	1.965 ± 0.005
	non-QCD	1000 ± 100	300 ± 17	190 ± 20	

Table 2.7: QCD background estimation as a function of the analysis selections for b-veto category. The yields for the different control regions, as well as the scaling factor R_{QCD}, are reported. The error on the R_{QCD} is statistical only.
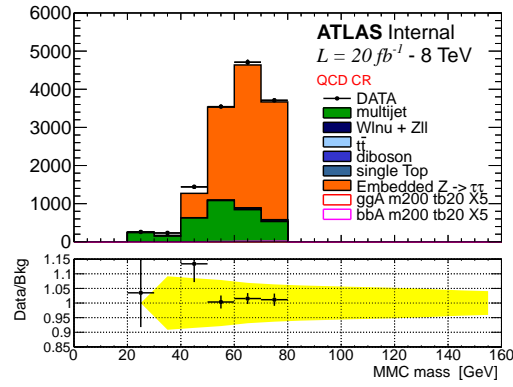
(a)
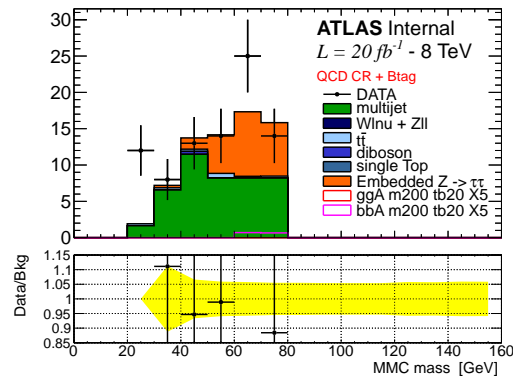
(b)

Figure 2.11: MMC_{mass} distribution for QCD cross check regions defined in section 2.2.3 (a) and for the same CR when in addition one b-tagged jet is required (b).
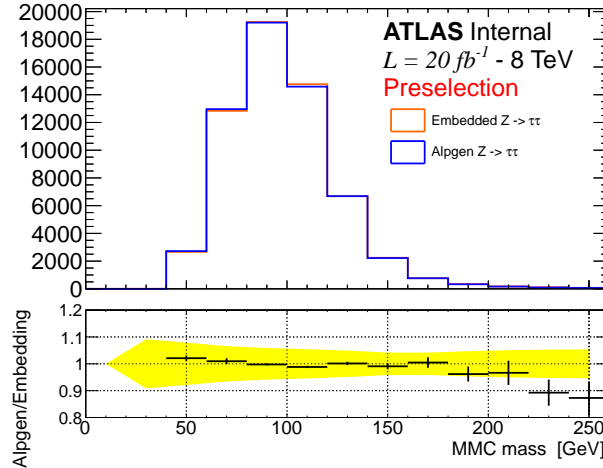
Figure 2.12: Comparison between the embedded $Z \rightarrow \tau\tau$ and ALPGEN for MMC_{mass} distributions.

reconstruction efficiency, then trigger and reconstruction efficiency for a $e - \mu$ final state are emulated by means of event weight.

The Embedding technique has been validated in several studies, detailed in [40, 42], which show a good description of data and $Z \rightarrow \tau\tau$ MC by Embedding. In the context of this analysis, figures 2.12 and 2.13 show comparisons of various kinematic variables between data, embedding and ALPGEN $Z \rightarrow \tau\tau$ events at preselection. No significant deviation is seen between the MMC_{mass} distribution of the embedding and ALPGEN samples, however other relevant variables for this analysis, such as the E_T^{miss} and the number of b-jets, are slightly better described by embedding.

The Embedding sample is based on selecting $Z \rightarrow \mu\mu$ candidates in data, the selections assure a rather pure $Z \rightarrow \mu\mu$ sample, however further selections used in this analysis, for example the b-tagging requirements, could enhance the contamination fraction from other processes. Dedicated studies have been made to estimate the $t\bar{t}$ and QCD multi-jet contamination in the embedding sample. The $t\bar{t}$ contamination is estimated by evaluating the embedding yield in a two b-tag control region (as described in Section 2.2.2), these events are assumed to be solely from $t\bar{t}$ and their yield in the signal region is extrapolated using MC simulation. Table 2.8 shows a summary for the top contamination in embedding The multi-jet contamination can be estimated starting from the embedding yield in (ABCD) region C, assuming all events in this CR as QCD multi-jet events, the contamination in the SR can be estimated by means of the ABCD method (see Section2.2.3). The R_{QCD} factor, in this case, is evaluated using a $\mu - \mu$ final state with same kinematic selections as for embedding $Z \rightarrow \mu\mu$ candidate. Table 2.9 shows the estimated contamination of QCD multi-jet in embedding. We consider contamination effects negligible.
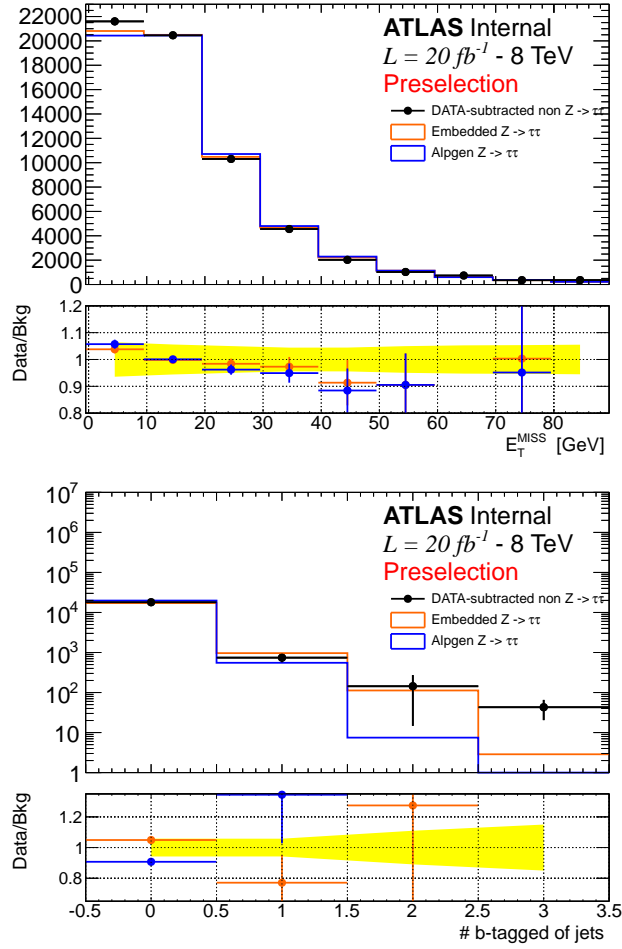
Figure 2.13: Comparison between embedded $Z \rightarrow \tau\tau$ and ALPGEN for E_T^{miss} and the number of b-tagged jets distributions. Data are superimposed, with the contribution of non-$Z \rightarrow \tau\tau$ are subtracted.

	Embedding yield in CR	Transfer factor	Estimated events in SR	Contamination
b-tag	84 ± 9	$(2.6 \pm 0.1) \times 10^{-2}$	2.2 ± 0.2	0.5 %
b-veto	84 ± 9	$(1.74 \pm 0.02) \times 10^{-1}$	15 ± 2	0.03 %

Table 2.8: Evaluating embedding $t\bar{t}$ contamination using a two b-tag CR. The transfer factor is the multiplicative factor that allows to estimate events in SR from the CR.

	Embedding yield in CR	Transfer factor	Estimated events in SR	Contamination
B-tag	12 ± 3	$(7 \pm 1) \times 10^{-3}$	$(8.4 \pm 0.3) \times 10^{-2}$	0.03 %
B-veto	390 ± 20	$(2.5 \pm 0.1) \times 10^{-2}$	10.0 ± 0.5	0.02 %

Table 2.9: Evaluating embedding contamination due to QCD multi-jet using ABCD method, the CR here is with OS anti-isolated events (region C). The transfer factor is the multiplicative factor that allows to estimate events in SR from the CR, in this case is N_B/N_D and is evaluated using mu-mu final state with the same kinematic selection used in the definition of the embedding sample.

2.3   Systematic Uncertainties

This section describes the range of systematic uncertainties that are relevant for this analysis. To account for differences in the detector responses between simulation and data a set of corrections are applied either at object reconstruction level and at event level, the uncertainties on such corrections are considered as detector-related systematic uncertainties and are detailed in section 2.3.1. For samples which rely on MC simulation, theory-related systematics, which include uncertainties on the cross-section and uncertainties on the acceptance of analysis selections, are described in section 2.3.2. Further systematic uncertainties related to data-driven methods for backgrounds estimation are described in section 2.3.3 and 2.3.4.

Each single systematic can contribute separately to the uncertainty on the final event yield and on the shape of the MMC_{mass} distribution which is used as discriminating variable in limit derivation. Shape systematics are documented in appendix ??, they are found to be negligible for all the samples except Embedding, for which significant deviation are found only in the b-veto category. Systematic uncertainties that do not effect the mass shape distribution and have an impact on the event yield of less than 0.5% (per sample) are neglected in the final limit calculations.

2.3.1   Detector-related Systematics Uncertainties

Here systematic uncertainty related to object reconstruction and event corrections are addressed, those corrections are based on the measure of some relevant parameter, each of those parameters correspond to a "nuissance paremeter" in our probability model as described in Section ??. Each parameter is varied independently (one sigma up or down) according with its uncertainty and the impact on the analysis yield for each sample is evaluated. In the following, detector related uncertainty are described with some more details, table 2.10 and 2.11 briefly summarize the impact on the samples yield for the most significant systematic uncertainty considered.

Luminosity   The integrated luminosity of the 8 TeV data recorded at ATLAS during 2012 is measured to be 20.3 fb^{-1} [66], its uncertainty is 2.8%.

Pileup Simulated events are re-weighted to reproduce the average interactions per bunch crossing, $< \mu >$, seen in data. Those event weights has an uncertainty wich is propagated to each simulated sample.

Trigger Efficiency is corrected in simulation to match (as a mean value) the one in data, those correction weights are evaluated as a function of p_t and η of the leptons and have assciated uncertainties. Systematic uncertainties on both the single electron and electron-muon trigger efficiency are considered independently, those uncertainty range aproximately 1-2%.

In the embedding sample, the trigger is emulated by applying weights to the event topology in order to recover the right trigger efficiency, those weights are related to the one just described above and have similar uncertainty. Trigger efficiency uncertainty for Embedding are considered uncorrelated with the one of other samples.

Electrons Two types of uncertainty on reconstructed electron objects are considered: the first are related to electron identification and reconstruction efficiencies ("Electron ID"), the second type are related to electron energy scale and resolution corrections. The energy scale uncertainties are split into a set of six different nuisance parameters, however, only few of them give a non negligible contribution. Two of them are found to effect the shape of the MMC_{mass} distribution and are considered independently, those are the uncertainty that arise from the $Z \rightarrow ee$ momentum measurement ("Electron Zee") and the one related to low momentum electrons ("Electron LOWPT"). All the other uncertainties related to energy scale and resolution are summed in quadrature ("Electron E").

Muons The uncertainty on muon identification efficiency depends on the charge and momentum of the muon. Typically these uncertainties are of the order of a fraction of percent, and are referred as "Muon ID". The uncertainties on the muon energy scale and resolution are considerd independently for the inner detector and muon spectrometer measurements, then are added in quadrature to eastimate the final effect ("Muon E").

Taus Hadronic tau object are only used in the analysis as a veto. Uncertainties on both tau energy scale and identification efficiency have been investigated and are found to be negligible for this analysis.

Jets The systematic uncertainties on the Jet Energy Scale (JES) are split up into multiple sets of nuisance parameters, which are related to different effects and components, for example the sensitivity to pileup or to the flavour composition of the jet. The overall uncertainty on the JES ranges between 3% and 7%, depending on the p_t and η of the jet. To give an idea of the effect that these uncertainty have on the analisis yield their sum in quadrature is reported in table 2.10 and 2.11 as "JES", however this is just a simplification for illustration purposes and in the limits extraction those uncertainties are considered uncorrelated. Systematic uncertainty

b-tag category uncertainties (%)				
Source	Signal bbH	Signal ggH	$Z \to \tau\tau$	Top	Other
Electron ID	2.3	2.6	2.8	1.8	2.0
Electron E	0.7	1.2	0.5	0.5	0.9
Electron LOWPT	0.4	0.0	0.4	0.1	0.4
Electron Zee	0.3	0.6	0.4	0.6	0.5
Muon ID	0.3	0.3	0.3	0.3	0.3
Muon E	0.5	0.8	0.1	0.1	0.2
Trigger Single Ele.	0.7	0.5	0.5	0.8	0.8
Trigger Dilepton	1.0	1.2	1.4	0.6	0.6
Embedding MFS	-	-	0.0	-	-
Embedding Iso.	-	-	1.3	-	-
JES	2.7	7.3	-	10.0	7.0
JER	1.4	6.3	-	2.9	3.0
B Eff	10.2	3.1	-	2.6	5.0
C Eff	0.2	4.3	-	0.0	1.2
L Eff	0.4	8.0	-	0.1	1.2
Pileup	0.4	0.7	0.4	0.4	0.9
MET	0.7	0.5	0.2	1.0	1.2
Luminosity	2.8	2.8	2.8	2.8	2.8

Table 2.10: Summary of the effect of the experimental systematic uncertainties on the yields of the different samples used in the b-tag channel. Here "Other" refers to the sum of all the remaining samples: $W \to \ell\nu$, diboson, $Z \to \ell\ell$ and single top. The signal samples listed here are b-associated production and gluon fusion with $m_A = 120$ GeV and $\tan\beta = 20$.

due to jet resolution ("Jet Resolution") are obtained by smearing the jet energy according to its uncertainty.

b-Tagging   is described in chapter **??**. Corrections are applied to simulation to match b-tagging efficiency in data, uncertainties on the knowledge of the b-tagging efficiencies for the 70% working point of the MV1 b-tagger are considered. The effect of those uncertainties is evaluated independently in the cases of b-quark, c-quark and light or gluon initiated jets and referred respectively to as "B Eff", "C Eff" and "L Eff". The tagging and mistagging efficiency uncertainties are considered to be totally anti-correlated.

Missing Transverse Energy   The effect of the energy scale uncertainties for all the physics objects is propagated to the E_T^{miss} calculation. In addition uncertainty on the energy scale and resolution due to the remaining calorimeter energy deposit, the so called "soft-terms", are considered. All the uncertainty on E_T^{miss} are independently propagated through the analysis and are added in quadrature, this final term is referred as "MET" uncertainty.

b-veto category uncertainties (%)					
Source	Signal bbH	Signal ggH	$Z \to \tau\tau$	Top	Other
Electron ID	2.4	2.3	2.9 (**s**)	1.4	1.6
Electron E.	0.4	0.5	0.4	0.5	0.9
Electron LOWPT	0.3	0.5	0.4 (**s**)	0.0	1.2
Electron Zee	0.4	0.4	0.4 (**s**)	0.1	0.3
Muon ID	0.3	0.3	0.3	0.3	0.3
Muon E.	0.1	0.1	0.1	0.5	0.5
Trigger Single Ele.	0.6	0.6	0.5	0.9	0.9
Trigger Dilep.	1.0	1.0	1.3	0.2	0.3
Embedding MFS	-	-	0.1 (**s**)	-	-
Embedding Iso.	-	-	0.0 (**s**)	-	-
JES	0.6	0.7	-	1.0	1.2
JER	0.5	0.3	-	0.6	0.3
B Eff	1.8	0.0	-	12.0	0.8
C Eff	0.0	0.1	-	0.1	0.0
L Eff	0.0	0.1	-	0.2	0.1
Pileup	0.5	0.8	0.4	0.3	0.3
MET	0.2	0.8	0.1	0.2	0.5
Luminosity	2.8	2.8	2.8	2.8	2.8

Table 2.11: Summary of the effect of the experimental systematic uncertainties on the yields of the different samples used in the b-veto channel. Here "Other" refers to the sum of all the remaining samples: $W \to \ell\nu$, diboson, $Z \to \ell\ell$ and single top. The signal samples listed here are b-associated production and gluon fusion with $m_A = 120$ GeV and $\tan\beta = 20$. Shape uncertainty are noted with the symbol (**s**).

2.3.2 Theoretical Uncertainties

Uncertainties on the cross-sections that have been used to normalise simulation samples to data are reported in Table 2.13. These uncertainties include contributions due to parton distribution functions (PDFs), the choice of the value of strong coupling constant, and the renormalisation and factorisation scales. Furthermore the uncertainties on signal cross-section depends on $\tan\beta$, the Higgs boson type $(A/h/H)$ and mass.

The effect of systematic uncertainties due to various MC tuning parameters, underlying event and lepton kinematic description is considered. Since the effect on the invariant mass distribution of the di-tau system from these systematic uncertainties is negligible (as an example see Figure 2.14), only the variation in acceptance is considered as systematic uncertainty. The acceptance uncertainties for the ALPGEN Z MC, used for the normalisation of the embedded sample, are estimated at lepton preselection to be 4% [64]. Since additional selections are applied directly to the embedded sample, no further acceptance uncertainties is considered. Acceptance systematics on $t\bar{t}$ simulated events are estimated to be of 2%. The acceptance uncertainties on diboson and single top production are assumed to be 2%. Uncertainties on signal acceptance have been estimated by producing samples with varied MC generator parameters and evaluating, at truth-level, the effect of analysis selections on leptons, taus and jets. This truth-level study is implemented within the Rivet framework [68], where additionally b-tagging is performed by identifying b-quarks and applying a weighting according to the estimated ATLAS b-tagging efficiencies [65]. The variation of the acceptance with respect to the nominal MC tune has been considered as a source of systematic uncertainty. For signal a total acceptance uncertainty varies from 4% to 30% depending on m_A, production process and on the analysis category.

2.3.3 $Z \to \tau\tau$ Embedding Systematics

An important element of the embedding method is the subtraction of the calorimeter cells associated with the muons in the original $Z \to \mu\mu$ event and their substitution with those from the simulated tau decays. To make a conservative estimate of the systematic uncertainty on this procedure, the energy of the subtracted cells is scaled up or down by 30%. The analysis is repeated with those modified samples and the relative uncertainty is referred as "EMB_MFS", this uncertainty affects mainly the shape of the MMC_{mass} distribution, shown in figure 2.15.

In the selection of the $Z \to \mu\mu$ sample only a loose requirement on muon track isolation is required. A different selection on the muon isolation may effect the selected sample by modifying the topology of the event, changing the non-$Z \to \mu\mu$ contamination or the activity in the calorimeter. To estimate the importance of these effects in our embedding sample, the isolation selection on the muons in the original $Z \to \mu\mu$ events is tightened, a looser selection would have limited impact because of isolation requirements at trigger level. The resulting uncertainty, referred to as "EMB_ISO", affects both the yield and the MMC_{mass} shape of the embedding samples, as shown in figure 2.15.

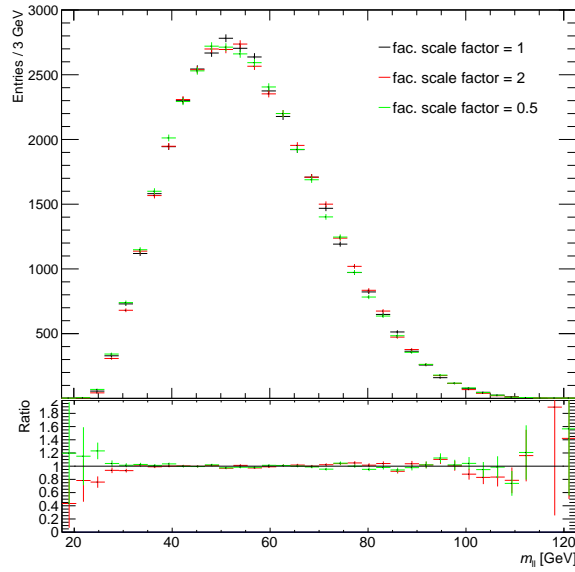Finally, because the normalisation of the embedding sample is determined by the

Figure 2.14: Comparison of the visible mass of tau decay products after factorisation scale variation for the b-veto category on a gluon fusion signal sample.
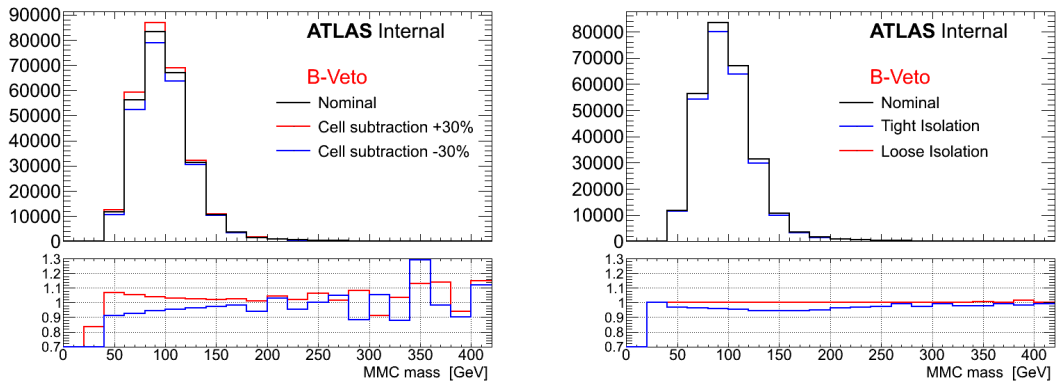

Figure 2.15: Impact of EMB_MFS (left) and EMB_ISO (right) systematic uncertainties MMC_{mass}distribution for Embedding sample. Only the b-veto category report significant deviations.

use of the ALPGEN sample, the relative cross section and luminosity uncertainties are assigned. In addition all the detector-related systematic uncertainties relevant to the decay products of the simulated tau decay are propagated to the embedding sample.

2.3.4   QCD Multi-Jet Systematics

In this analysis the QCD multi-jet background is estimated via the ABCD method, as described in Section 2.2.3. This technique relies strongly on the assumption that the lepton isolation variables are independent from the charge correlation between the two leptons. Systematic uncertainties are assigned to take into account deviations from this assumption. First the correlation between R_{QCD} and the lepton isolation selections is considered, then the result is compared with an auxiliary method.

Figure 2.16 shows the R_{QCD} factor, the ratio between the QCD yields in region C and D, as a function of the lepton isolation selections (red points). As described previously, the expectation from non-QCD backgrounds is subtracted from the data in regions C and D. To estimate the uncertainty on the value of R_{QCD} an additional transfer factor is defined as follows: $R_{QCD}^{iso} = \hat{A}/\hat{B}$, where $\hat{A}$ and $\hat{B}$ are semi-isolated OS and SS regions defined with the lepton isolation larger than the standard requirement, but less than a sliding cut. Once more, the non-QCD contributions are subtracted from the data yields. The regions $\hat{A}$ and $\hat{B}$ are chosen to be semi-isolated due to the high contamination of non-QCD background and possible signal in region A and B. Figure 2.16 shows R_{QCD}^{iso} as a function of the lepton isolation selections (black points). The difference between R_{QCD} and R_{QCD}^{iso} in the vicinity of the standard cut value is then assigned as a systematic uncertainty on R_{QCD}. Using the point where the cuts on the lepton isolation are twice their standard values, a systematic uncertainty of 15% is found. The plot in Figure 2.16 is made at preselection level, similar plots using the full selection for the two categories are in Appendix B.

An additional method, used as a crosscheck, considers calculating R_{QCD} as the ratio between the estimated QCD contributions in region A and B. Here the non-QCD contributions are once more subtracted from data. However the large contribution of this non-QCD background, along with lack of statistics and possible signal contamination, lead to this method being only used as a cross check. Table 2.12 shows a comparison between R_{QCD} and R_{QCD}^{AB} for the two categories at the preselection stage of the cutflow, where signal contamination is negligible. Agreement is seen between R_{QCD} values in the two regions, within statistical uncertainties.

The difference in MMC_{mass} shape observed between the OS and SS anti-isolated regions (C and D) is shown in Figure 2.17. This effect is within the uncertainty on R_{QCD} of the ABCD method, hence no correction factor is applied to the mass shape. We assume, however, that there could be the same shape difference in the isolated regions, a shape uncertainty is then assigned to region B to take into account this deviation. Further shape uncertainties due to non-QCD background subtraction are found to be negligible. The uncertainty due to the use of an isolation requirement at trigger level is discussed in Appendix A and is found to be negligible.

Selection	R_{QCD}	R_{QCD}^{AB}	R_{QCD}^{iso}
Preselection	1.929 ± 0.004	2.12 ± 0.17	2.22 ± 0.16
B-veto	1.965 ± 0.005	2.10 ± 0.16	2.22 ± 0.16
B-tag	1.78 ± 0.02	1.9 ± 0.9	2.0 ± 0.8

Table 2.12: Comparison between R_{QCD}, R_{QCD}^{AB} and R_{QCD}^{iso} for early stage in the cutflow, only b-tag and b-veto requirement are applied after preselections. Reported is statistical uncertainty only.
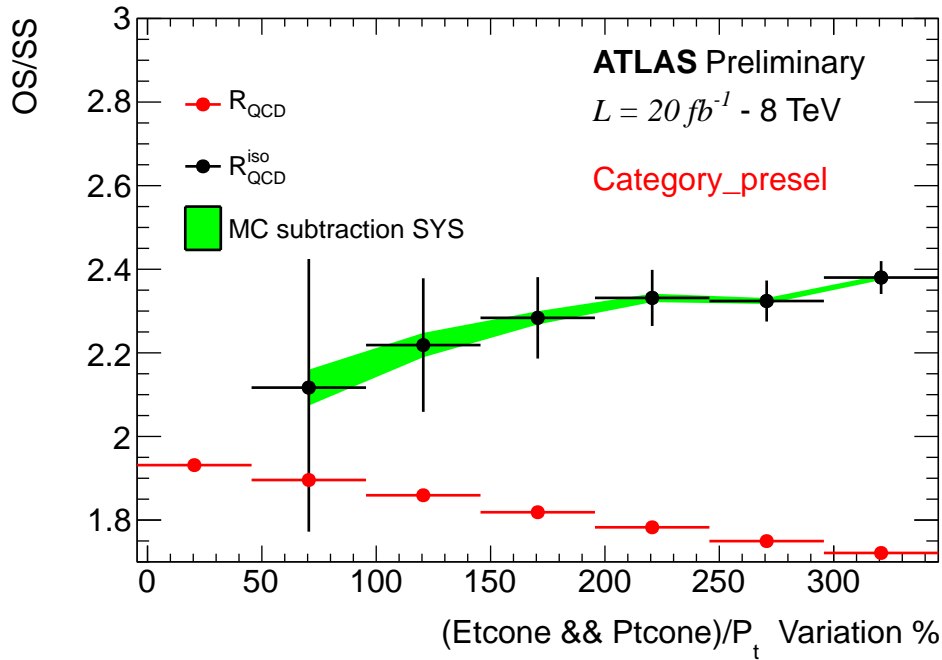

Figure 2.16: OS/SS ratio as a function of lepton isolation variable selections. The selections are varied as a percentage relative to the standard lepton isolation cut values (0 in the plot). The red points show the anti-isolated scale factor R_{QCD}, i.e. the ratio between regions C and D. The black points show the isolated scale factor, which is defined as the ratio between region $\hat{A}$ and $\hat{B}$, where the leptons have isolation values larger than the nominal value but smaller than the sliding cut on X axis.
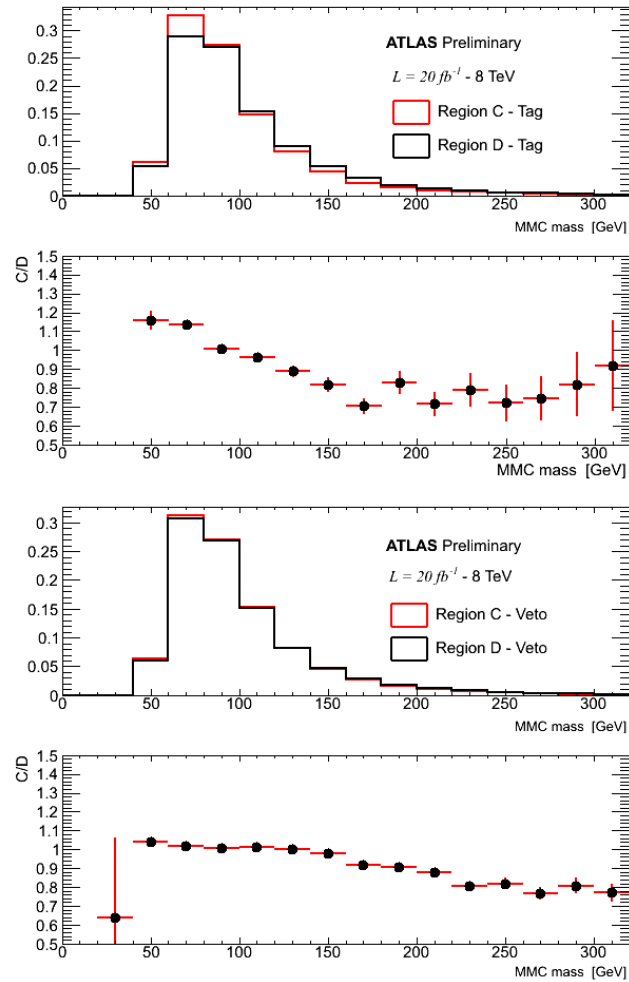
Figure 2.17: Shape differences for the b-tag and b-veto categories between the ABCD regions C and D.

Generator	Process	Uncertainty
ALPGEN	$Z \to \tau\tau/ee/\mu\mu$	$\pm 5\%$
POWHEG	$t\bar{t}$	$\pm 5.5\%$
ALPGEN	$W \to \tau\nu/e\nu/\mu\nu$	$\pm 5\%$
AcerMC	single top	$\pm 13\%$
HERWIG	dibosons	$\pm 6\%$
SHERPA	$bbA/h/H$ ($m_A \geq 120$ GeV)	$-(< 20)\%, +(< 9)\%$
SHERPA	$bbA/h/H$ ($m_A = 110$ GeV)	$-(< 25)\%, +(< 9)\%$
SHERPA	$bbA/h/H$ ($m_A = 100$ GeV)	$-(< 28)\%, +(< 9)\%$
SHERPA	$bbA/h/H$ ($m_A = 90$ GeV)	$-(< 30)\%, +(< 9)\%$
POWHEG	$ggA/h/H$ ($m_A \leq 300$ GeV)	$< 15\%$

Table 2.13: Cross-section uncertainties for background and signal samples. The reported signal samples are all for $\tan\beta = 20$.

2.4 Results

2.4.1 LHC Procedure For Limits Setting

A detailed description of the LHC procedure for Higgs search can be found in [?, ?], in the following a brief summary is given. Statistical tests are used for quantify an observation or to set an exclusion limit, in search for new phenomena, hypotesis testing is performed by means of two hypotesis: the *background only* H_0 and and the *signal+background* H_1. As its has allready been outlined in section 2.1.2, any statistical test is based on probability distribution, once a probability density function (p.d.f.) is defined, one can calculate its value for a given set of data obtaining what is called a "likelihood". Taking the marked Poisson p.d.f. in equation (2.1) one obtain the following likelihood function:

$$\mathcal{L}(\text{data}|\mu, \boldsymbol{\theta}) = \text{Poisson}(\text{data}|\mu \cdot s(\boldsymbol{\theta}) + b(\boldsymbol{\theta})) \cdot f(\boldsymbol{\theta}|\hat{\boldsymbol{\theta}}) \tag{2.3}$$

this now describes how likely are the data under a certain hypotesis and it is only function of the parameter μ and of the nuissance parameter $\boldsymbol{\theta}$. If the hypotesis under test is unlikely to happen with the given dataset the value of $\mathcal{L}$ is decreasing, one can define which is the best value of a parameter that describes the data via maximising the likelihood, obtaining a so called maximum likelihood estimator. The Poisson distribution in equation (2.3) stands for a product of Poisson probabilities to observe events in the bin i of an histogram:

$$\prod_i \frac{(\mu s_i + b_i)^{n_i}}{n_i!} \, e^{-\mu s_i - b_i}$$

while the $f(\boldsymbol{\theta}|\hat{\boldsymbol{\theta}})$ is the p.d.f. for a given set of nuissance parameter $\boldsymbol{\theta}$ with their best estimate $\hat{\boldsymbol{\theta}}$.

To compiute the compatibility of the data with the H_0 and H_1 hypotesis and then exclusion limits, one needs to define a test statistic. The test statistic, which has already been mentioned in section 2.1.2, is a function of the data which returns
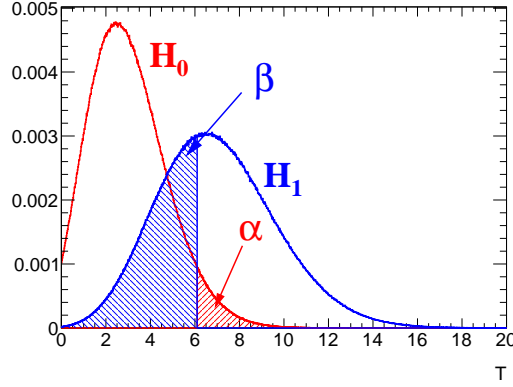
Figure 2.18: Example of a test statistic which in this case is just the total number of events of a counting experiment. Under the hypotesis H_0 are expected four events, while under the H_1 seven events are expected.

a real value. One can in principle use any test statistic, however, given the size of the test (probability to reject the null hypotesis when is true) one would like to have a test statistic which has the highest power $1 - \beta$ possible (probability to reject the null hypotesys when it is false). Figure 2.18 shows an example of the distribution of an hipotetical test statistic for two hypotesis. It has been shown by Neuman-P [] that in case of simple hyptesis (probability model without any parameter), then the test statistic with the highest power is the ratio of the likelihood calculated with the two hypotesis. The standard procedure at the LHC is to use the following test statistic [] based on the likelihood ratio:

$$\tilde{q}_\mu = -2\ln \frac{\mathcal{L}(\text{data}|\mu, \hat{\boldsymbol{\theta}}_\mu)}{\mathcal{L}(\text{data}|\hat{\mu}, \hat{\boldsymbol{\theta}})} \quad \text{with the constraint} \quad 0 \le \hat{\mu} \le \mu$$

where $\hat{\mu}$ and $\hat{\boldsymbol{\theta}}$ are the maximum likelihood estimators for μ and $\boldsymbol{\theta}$ given the data, whereas $\hat{\boldsymbol{\theta}}_\mu$ is the maximul likelihood estimator of $\boldsymbol{\theta}$ given the data but considering a signal streght of value μ, $\tilde{q}_\mu$ is increasing with increasing disagreement between data and the μ hypotesis under test. The procedure for limits setting follows five steps:

1. The signal hypotesis with signal streght μ is assumed, under this assumpion a set of *pseudo-data* is generated for different values of μ.

2. $\tilde{q}_\mu$ is calculated for each of the *pseudo-dataset* and each signal hypotesis generating the expected probability density function for $\tilde{q}_\mu$ given μ, $f(\tilde{q}_\mu \mid \mu, \hat{\boldsymbol{\theta}}_\mu, H_1)$.

3. One does the same thing for the null hypotesis, generate pseudo-data with the distribution of background only and obtain the $f(\tilde{q}_\mu \mid \mu = 0, \hat{\boldsymbol{\theta}}_0, H_0)$.

4. Once the p.d.f. for the signal and signal + background hypotesis is obtained, one can define for a given dataset (that can be this time real data or again pseudodata) two p-values for any given value of μ, which are the probability

to obtain data less compatible with the hypotesis in consideration:

$$p_{s+b} = P(\tilde{q}_\mu > \tilde{q}_\mu{}^{observed} \mid H_1)$$

$$p_b = P(\tilde{q}_\mu > \tilde{q}_\mu{}^{observed} \mid H_0)$$

The ratio of this two probability is what is called the $CL_s = p_{s+b}/p_b$ [].

5. If for a given μ is obtained $CL_s \leq \alpha$ one states that the signal hypotesis (with that μ) is excluded with (1 - α) CL_s confidence level. To get the 95% confidence level upper limit on μ, denoted as μ^{95} one adjust μ until $CL_s = 0.05$.

This is a quite complicated prescription, however its interpretation is not so different from the usual Neyman Costruction [] of confidence intervals: for each μ is possible to define $\tilde{q}_\mu{}^{95}$ for which the probability $\mathrm{P}(\tilde{q}_\mu \geq \tilde{q}_\mu{}^{95} \mid \mu,\ H_1) = 5\%$, this means that if H_1 is true one expects $\tilde{q}_\mu \geq \tilde{q}_\mu{}^{95}$ in 5% of the cases. With this definition μ^{95} would be the value of μ that for the observed data gives $\tilde{q}_\mu = \tilde{q}_\mu{}^{95}$, or in other words a p-value of 5%. By costruction, rejecting $\mu > \mu^{95}$ the hypotesis H_1 will be rejected, when is true, at most 5% of the time, given the fact that $\tilde{q}_\mu$ is increasing with increasing discrepancy of the hypotesis with data. The difference with the CL_s prescription is that there the ratio of p-values is used to define μ^{95}: it has been shown that this choice protect the upper limit from down fluctuation of the data, giving a conservative estimate in any case.

The expected median exclusion upper-limit and its error are evaluated by generating a large sample of *bacground only* pseudo-data and calculating CL_s and μ^{95} for each of them, from the distribution of μ^{95} one can get the mean excluded value and its error.

The actual implementation in the limit framework of the ABCD method follows that suggested in [62]. Here three free parameters are fitted: number of multi-jet events in region B, N_B^{QCD}, factor that extrapolates from SS region to OS regions, R_{QCD}, and the factor that extrapolates from isolated to anti-isolated regions R_{BD}. Neglecting signal contributions, the following equations can be written for the event yield of the B,C and D control regions:

$$N_B = N_B^{BKG} + N_B^{QCD}$$

$$N_C = N_C^{BKG} + N_B^{QCD} \times R_{QCD} \times R_{BD}$$

$$N_D = N_D^{BKG} + N_B^{QCD} \times R_{BD}$$

where N^{BKG} represent the prediction of non-QCD background in the relative regions. The estimate of multi-jet event yield in SR will be then $N_B^{QCD} \times R_{QCD}$. This method is particularly powerful because in the best fit of R_{QCD} the statistical and systematics uncertainty for non-QCD backgrounds and data will be considered.

Sample	b-tag category			b-veto category		
	N(event)	Stat.	Syst.	N(event)	Stat.	Syst.
$Z \to \tau\tau$	418	$\pm$ 6		54680	$\pm$ 60	
$t\bar{t}$	330	$\pm$ 10		2228	$\pm$ 25	
Multijet	100	$\pm$ 15		3940	$\pm$ 330	
$W \to \ell\nu$	10	$\pm$ 6		650	$\pm$ 100	
Diboson	13.1	$\pm$ 1.8		2921	$\pm$ 27	
Single Top	90	$\pm$ 6		443	$\pm$ 15	
$Z \to \ell\ell$	0.9	$\pm$ 0.8		430	$\pm$ 40	
Total	962	$\pm$ 16		65290	$\pm$ 180	
Signal						
Data	-	-	-	-	-	-

Table 2.14: Comparison between yield in data and the one expected from our background model, b-tag and b-veto category are reported separately.

2.4.2   Exclusion Limits

The procedure described in section 2.4.1 is the one used for the SM Higgs, for the MSSM further complication arises: one has to consider in the signal model three Higges, in a particular scenario the masses and cross section are defined for a given point in the $\tan\beta - m_A$ plane, so the procedure described previously has to be repeated for each point in that plane. For the m_h^{max} scenario exclusion limits are derived by calculating 95% CLs limits on the cross section of $bb/gg \to A/H/h \to \tau_{lep}\tau_{lep}$ for 15 $\tan\beta$ values (between[2] $\tan\beta = 5$ and $\tan\beta = 60$), a point in the $\tan\beta - m_A$ plane is excluded if $\mu^{95} \leq 1$ for that point, a linear interpolation is used to determine the $\tan\beta$ excluded for a given m_A. The procedure is followed for a set of different CP-odd Higgs masses m_A: 90, 100, 110, 120, 125, 130, 140, 150, 170, 200, 250 and 300 GeV. The event yield has been compared between data and background expectation in bins of the MMC_{mass} distribution. The bin sizes were chosen such that there are enough events left for the asymptotic approximation [69] to hold. Table 2.14 compares yields between data and background model for the two categories at the final stage of the cut flow. Additionally, figure 2.19 shows the MMC_{mass} distributions for the full b-tag and b-veto categories.

The resulting exclusion limit on the MSSM parameter space (m_A vs $\tan\beta$ plane) are interpreted within the m_h^{max} benchmark scenario [34] and shown in Figure C.12. The expected and observed 95% confidence-level limits are shown as solid and dashed black lines, the green and yellow bands correspond to the 1σ and 2σ error bands. The analysis is sensitive to MSSM Higgs production of $\tan\beta \geq 13$ for the range $90 < m_A < 200$ GeV. The observed limit is presently unknown.

The outcome of the search is also interpreted in the generic case of a scalar boson produced in the $pp \to gg \to \phi$ or $pp \to bb\phi$ mode and decaying to a di-tau pair. These limits are shown in Figure 2.21 for the b-associated and the gluon-gluon

---

[2]The set of $\tan\beta$ values used is 5, 8, 10, 13, 16, 20, 23, 26, 30, 35, 40, 45, 50, 55, 60
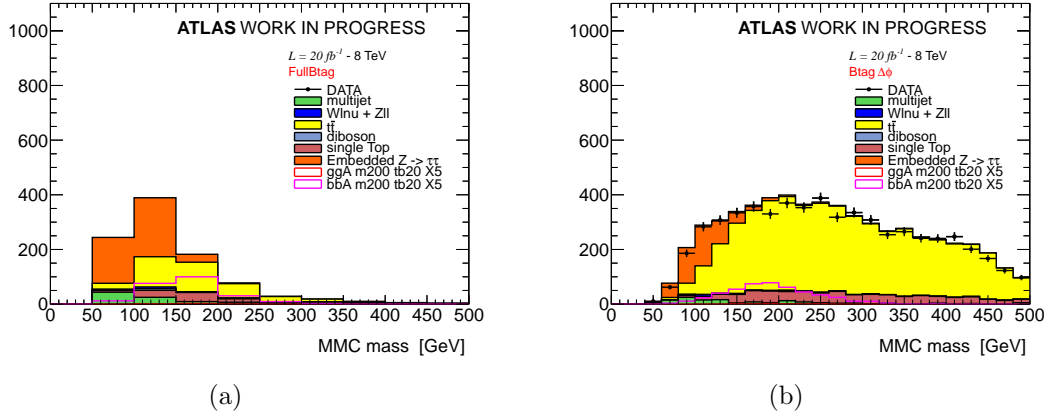
Figure 2.19: Distributions of the MMC_{mass} mass for (a) the full b-tag category selection and (b) the full b-veto selection.

fusion production mechanisms separately. All signal systematic uncertainties are implemented in the likelihood for this limit derivation, more information about the limits and their validation can be found in Appendix C.
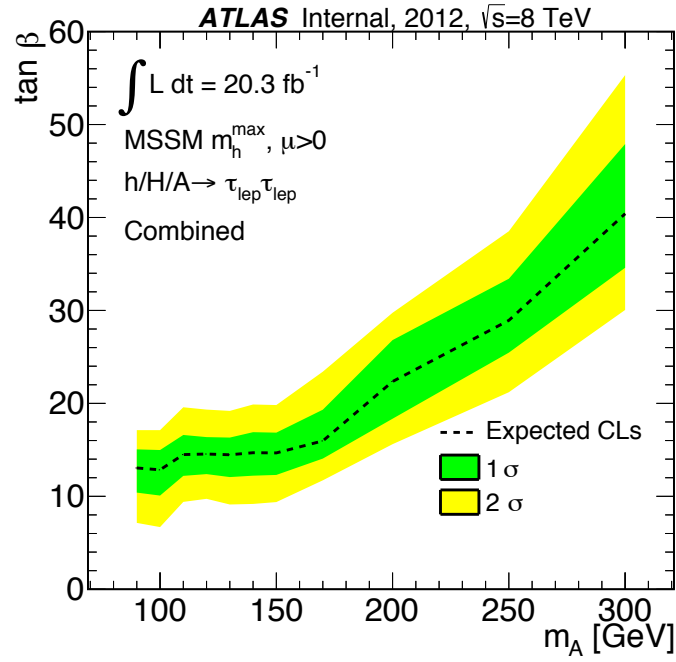
Figure 2.20: Expected exclusion limits for MSSM Higgs boson production in the MSSM m_A vs $\tan \beta$ parameter space.

Figure 2.21: Limits on the production of a scalar particle decaying to a di-tau pair and produced in association with b quarks (left) or via gluon-gluon fusion (right). Still not produced...

Bibliography

[1] L. Evans and P. Bryant, *LHC Machine*, JINST **3** (2008) S08001.

[2] F. Englert and R. Brout, *Broken Symmetry and the Mass of Gauge Vector Mesons*, Phys. Rev. Lett. **13** (1964) 321.

[3] P. W. Higgs, *Broken symmetries, massless particles and gauge fields*, Phys. Lett. **12** (1964) 132.

[4] P. W. Higgs, *Broken Symmetries and the Masses of Gauge Bosons*, Phys. Rev. Lett. **13** (1964) 508.

[5] P. W. Higgs, *Spontaneous Symmetry Breakdown without Massless Bosons*, Phys. Rev. **145** (1966) 1156.

[6] G. S. Guralnik, C.R. Hagen and T. W. B. Kibble Phys.Rev.Lett. **13** (1964) 585.

[7] N. P. Nilles, *Supersymmetry, supergravity and particle physics*, Phys. Rep. **110** (1984) 1.

[8] H. E. Haber and G. L. Kane, *The search for supersymmetry: Probing physics beyond the standard model*, Phys. Rep. **117** (1985) 75.

[9] ALEPH, DELPHI, L3 and OPAL Collaboration, *Search for neutral MSSM Higgs bosons at LEP*, Eur. Phys. J. **C47** (2006) 547.

[10] *Combined CDF and D0 upper limits on MSSM Higgs boson production in tau-tau final states with up to 2.2 fb^{-1} of data*, `arXiv:1003.3363 [hep-ex]`.

[11] CDF Collaboration, T. Aaltonen et al. Phys. Rev. Lett. **103** (2009) 201801.

[12] D0 Collaboration, V. Abazov et al. Phys. Rev. Lett. **101** (2008) 071804.

[13] TNPWG (Tevatron New Physics Higgs Working Group), CDF and D0 Collaborations, *Search for Neutral Higgs Bosons in Events with Multiple Bottom Quarks at the Tevatron*, `arXiv:1207.2757 [hep-ex]`.

[14] CDF Collaboration, T. Aaltonen et al., *Search for Higgs Bosons Produced in Association with b-quarks*, Phys.Rev. **D85** (2012) 032005, `arXiv:1106.4782 [hep-ex]`.

[15] D0 Collaboration, V.M. Abazov et al., *Search for neutral Higgs bosons in the multi-b-jet topology in 5.2fb^{-1} of p$\bar{p}$ collisions at $\sqrt{s} = 1.96$ TeV*, Phys.Lett. **B698** (2011) 97–104, `arXiv:1011.1931 [hep-ex]`.

[16] The CMS Collaboration, S. Chatrchyan et al., `arXiv:1104.1619 [hep-ex]` `[hep-ex]`.

[17] The ATLAS Collaboration , *Search for the neutral Higgs bosons of the Minimal Supersymmetric Standard Model in pp collisions at $\sqrt{s} = 7$ TeV with the ATLAS detector*, `arXiv:1211.6956 [hep-ex]`.

[18] T. A. Collaboration, *Observation of a new particle in the search for the Standard Model Higgs boson with the ATLAS detector at the LHC*, Physics Letters B **716** (2012) 1–29.

[19] T. C. Collatoration, *Observation of a new boson at a mass of 125 GeV with the CMS experiment at the LHC*, Physics Letters B **716** (2012) 30–61.

[20] S. Heinemeyer, O. Stål and G. Weiglein, *Interpreting the LHC Higgs search results in the MSSM*, Phys.Lett. **B710** (2012) 201–206, `arXiv:1112.3026 [hep-ph]`.

[21] A. Arbey, M. Battaglia, A. Djouadi and F. Mahmoudi, *The Higgs sector of the phenomenological MSSM in the light of the Higgs boson discovery*, JHEP **1209** (2012) 107, `arXiv:1207.1348 [hep-ph]`.

[22] The ATLAS Collaboration, G. Aad et al., *The ATLAS Experiment at the CERN Large Hadron Collider*, JINST **3** (2008) S08003.

[23] M. L. Mangano et al., *ALPGEN, a generator for hard multiparton processes in hadronic collisions*, JHEP **07** (2003) 001.

[24] J. Alwall et al., *Comparative study of various algorithms for the merging of parton showers and matrix elements in hadronic collisions*, Eur. Phys. J. **C53** (2008) 473, `arXiv:0706.2569`.

[25] S. Frixione and B. R. Webber, *Matching NLO QCD computations and parton shower simulations*, JHEP **06** (2002) 029, `hep-ph/0204244`.

[26] B. P. Kersevan and E. Richter-Was, *The Monte Carlo Event Generator AcerMC 2.0 with Interfaces to PYTHIA 6.2 and HERWIG 6.5*, `arXiv:0405247v1 [hep-ph]`.

[27] G. Corcella et al., *HERWIG 6: an event generator for hadron emission reactions with interfering gluons (including supersymmetric processes)*, JHEP **01** (2001) 010.

[28] J. M. Butterworth, J. R. Forshaw, and M. H. Seymour, *Multiparton Interactions in Photoproduction at HERA*, Z. Phys. **C72** (1996) 637.

[29] T. Binoth, M. Ciccolini, N. Kauer, and M. Kramer, *Gluon-induced W-boson pair production at the LHC*, JHEP **12** (2006) 046.

[30] A. S. et al., *Higgs boson production in gluon fusion*, JHEP **02** (2009) 029.

[31] T. Gleisberg et al., *Event generation with SHERPA 1.1*, JHEP **02** (2009) 007.

[32] J. Pumplin, D. R. Stump, J. Huston, H. L. Lai, P. M. Nadolsky and W. K. Tung, "New generation of parton distributions with uncertainties from global QCD analysis," JHEP **0207** (2002) 012 [hep-ph/0201195].

[33] H. -L. Lai, M. Guzzi, J. Huston, Z. Li, P. M. Nadolsky, J. Pumplin and C. -P. Yuan, "New parton distributions for collider physics," Phys. Rev. D **82** (2010) 074024 [arXiv:1007.2241 [hep-ph]].

[34] M. Carena, S. Heinemeyer, C. E. M. Wagner, and G. Weiglein, *Suggestions for benchmark scenarios for MSSM Higgs boson searches at hadron colliders*, Eur. Phys. J. **C26** (2003) 601–607, `hep-ph/0202167`.

[35] The ATLAS Collaboration, *ATLAS Monte Carlo Tunes for MC09*, ATL-PHYS-PUB-2010-002.

[36] S. Jadach, J. H. Kuhn and Z. Was, *TAUOLA - a library of Monte Carlo programs to simulate decays of polarized τ leptons*, Comput. Phys. Commun. **64** (1990) 275.

[37] E. Barberio, B. V. Eijk and Z. Was, *Photos - a universal Monte Carlo for QED radiative corrections in decays*, Comput. Phys. Commun. **66** (1991) 115.

[38] The GEANT4 Collaboration, S. Agostinelli et al., *GEANT4 - a simulation toolkit*, Nucl. Instrum. Meth. **A506** (2003) 250.

[39] The ATLAS Collaboration, G. Aad et al., *The ATLAS Simulation Infrastructure*, ATLAS-SOFT-2010-01-004, submitted to Eur. Phys. J. C., `arXiv:1005.4568`.

[40] The ATLAS Collaboration, *Estimation of $Z \to \tau\tau$ Background in VBF $H \to \tau\tau$ Searches from $Z \to \mu\mu$ Data using an Embedding Technique*, ATL-PHYS-INT-2009-109.

[41] The ATLAS Collaboration, *Search for the Standard Model Higgs boson in the $H \to \tau\tau$ decay mode with 4.7 fb1 of ATLAS detactor*, Tech. Rep. ATLAS-CONF-2012-014, CERN, Geneva, Mar, 2012.

[42] The ATLAS Collaboration, *Search for the Standard Model Higgs boson $H \to \tau\tau$ decays with the ATLAS detector*, ATL-COM-PHYS-2013-722.

[43] T. S. et al., Z *physics at LEP 1*, CERN 89-08 **3** (1989) 143.

[44] The ATLAS Collaboration, *Expected Performance of the ATLAS Experiment - Detector, Trigger and Physics*, CERN-OPEN-2008-020, `arXiv:0901.0512`.

[45] The ATLAS Collaboration, *ATLAS Muon Momentum Resolution in the First Pass Reconstruction of the 2010 p-p Collision Data at $\sqrt{s} = 7$ TeV*, ATLAS-CONF-2011-046.

[46] The ATLAS Collaboration, *Muon reconstruction efficiency in reprocessed 2010 LHC p-p collision data recorded with the ATLAS detector*, ATLAS-CONF-2011-063.

[47] The ATLAS Collaboration, *Expected electron performance in the ATLAS experiment*, ATLAS-PUB-2011-006.

[48] ATLAS egamma WG, *Electron efficiency measurements*, https://twiki.cern.ch/twiki/bin/view/AtlasProtected/EfficiencyMeasurements.

[49] M. Cacciari, G. P. Salam, and G. Soyez, *The anti-k_t jet clustering algorithm*, JHEP **04** (2008) 063.

[50] W. Lampl et al., *Calorimeter Clustering Algorithms : Description and Performance*, ATL-LARG-PUB-2008-002.

[51] T. Barillari et al., *Local Hadron Calibration*, ATL-LARG-PUB-2009-001.

[52] The ATLAS Collaboration, *Jet energy scale and its systematic uncertainty in proton-proton collisions at $\sqrt{s} = 7$ TeV in ATLAS 2010 data*, ATLAS-CONF-2011-032.

[53] TheATLAS Collaboration, *Performance of the Reconstruction and Identification of Hadronic tau Decays in ATLAS with 2011 Data*, ATLAS-CONF-2012-142.

[54] The ATLAS Collaboration, *Reconstruction and Calibration of Missing Transverse Energy and Performance in Z and W events in ATLAS Proton-Proton Collisions at $\sqrt{s}=7$ TeV*, ATLAS-CONF-2011-080.

[55] A. Elagin, P. Murat, A. Pranko, and A. Safonov, *A New Mass Reconstruction Technique for Resonances Decaying to di-tau*, `arXiv:1012.4686 [hep-ex]`. * Temporary entry *.

[56] ATLAS Jet/EtMiss Combined Performance Group, *Jet Energy Resolution Provider*, https://twiki.cern.ch/twiki/bin/view/Main/JetEnergyResolutionProvider.

[57] The ATLAS Collaboration, *Data-Quality Requirements and Event Cleaning for Jets and Missing Transverse Energy Reconstruction with the ATLAS Detector in Proton-Proton Collisions at a Center-of-Mass Energy of $\sqrt{s} = 7$ TeV*, ATLAS-CONF-2010-038.

[58] T. A. Collaboration, *Search for neutral MSSM Higgs bosons decaying to $\tau\tau$ pairs in proton-proton collisions at with the ATLAS detector*, Physics Letters B **705** (2011) no. 3, 174 – 192.

[59] The ATLAS Collaboration, *Data-driven estimation of the background to charged Higgs boson searches using hadronically-decaying tau final states in AT-LAS,* ATLAS-CONF-2011-051.

[60] The ATLAS Collaboration, *Measurement of the $Z \to \tau\tau$ cross section with the ATLAS detector*, Phys. Rev. D **84** (2011) 112006.

[61] T. A. Collaboration, *Search for the neutral Higgs bosons of the Minimal Supersymmetric Standard Model in pp collisions at $\sqrt{s} = 7$ TeV with the ATLAS detector*, JHEP , `arXiv:1211.6956`.

[62] Atlas statistics forum, *ABCD method in searches*, link

[63] The ATLAS Collaboration, *Search for Neutral MSSM Higgs Bosons H to $\tau\tau$ to $l\tau_h$ with the ATLAS Detector in 7 TeV Collisions*, ATL-COM-PHYS-2012-094.

[64] The ATLAS Collaboration, *Search for neutral Higgs Bosons in the decay mode $H \to \tau\tau \to ll+4\nu$ in proton proton collision at $\sqrt{7}$ TeV with the ATLAS Detector*, ATL-COM-PHYS-2011-758.

[65] The ATLAS Collaboration, *Measurement of the b-tag Efficiency in a Sample of Jets Containing Muons with 5 fb^{-1} of Data from the ATLAS Detector*, ATLAS-CONF-2012-043.

[66] The ATLAS Collaboration, *Luminosity Determination in pp Collisions at $\sqrt{s} = 7$ TeV using the ATLAS Detector in 2011*, ATLAS-CONF-2011-116.

[67] T. Sjostrand, S. Mrenna and P. Skands, *PYTHIA 6.4 physics and manual*, JHEP **05** (2006) 026.

[68] A. B. et al., *Rivet user manual*, `arXiv:1003.0694 [hep-ph]`.

[69] E. G. G. Cowan, K. Cranmer and O. Vitells, *Asymptotic formulae for likelihood-based tests of new physics*, `arXiv:1007.1727 [hep-ex]`.

[70] LHC Higgs Cross Section Working Group, S. Dittmaier, C. Mariotti, G. Passarino, R. Tanaka (Eds.), et al., *Handbook of LHC Higgs Cross Sections: 1. Inclusive Observables*, `arXiv:1101.0593 [hep-ph]`.

[71] LHC Higgs Cross Section Working Group, S. Dittmaier, C. Mariotti, G. Passarino, and R. Tanaka (Eds.), *Handbook of LHC Higgs Cross Sections: 2. Differential Distributions*, CERN-2012-002 (CERN, Geneva, 2012) , `arXiv:1201.3084 [hep-ph]`.

[72] D. de Florian, G. Ferrera, M. Grazzini and D. Tommasini, *Transverse-momentum resummation: Higgs boson production at the Tevatron and the LHC*, JHEP **1111** (2011) , `arXiv:1109.2109 [hep-ph]`.

[73] Statistical twiki, NuissanceCheck. https://twiki.cern.ch/twiki/bin/view/AtlasProtected/Nuisan

Appendix A

QCD Trigger bias

The single electron trigger (`EF_e24vhi_medium1`) used in this analysis includes the following isolation cut: $p_T(\text{cone})20/p_t < 0.1$. This means that the kinematical distributions in the anti-isolated ABCD regions will biased due to a reduced efficiency for high p_t electrons. This unwanted feature may potentially effect the R_{QCD} factor, as the OS/SS ratio may differ due to different p_t spectrum. To check the effect on R_{QCD} the ABCD method has been repeated using the `EF_e24vh_medium1` trigger, which doesn't include isolation and hence is prescaled in 2012 8 TeV data. The prescale of a factor around 100 has been taken in consideration using trigger information stored in D3PD. Figure A.1 shows $p_T(\text{cone})$ distribution for the standard and test triggers. The comparable event yields in the region $p_T(\text{cone})20/p_t < 0.1$ show that the prescale normalisation for the test trigger has been correctly accounted for.

Figure A.2 shows the behaviour of R_{QCD} factor as a function of isolation variable for the two triggers under test. As the deviations are within statistical uncertainty, we conclude that the isolation requirement used at trigger level does not influence the OS/SS ratio. Hence no further systematic uncertainty is assigned.
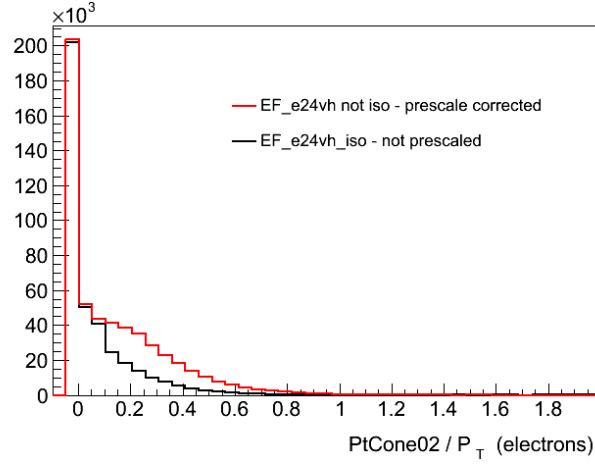
Figure A.1: $p_T(\mathrm{cone})$ / p_t distribution for the analysis standard trigger and its corrispective without isolation requirement, this second trigger is rescaled according to prescales information.
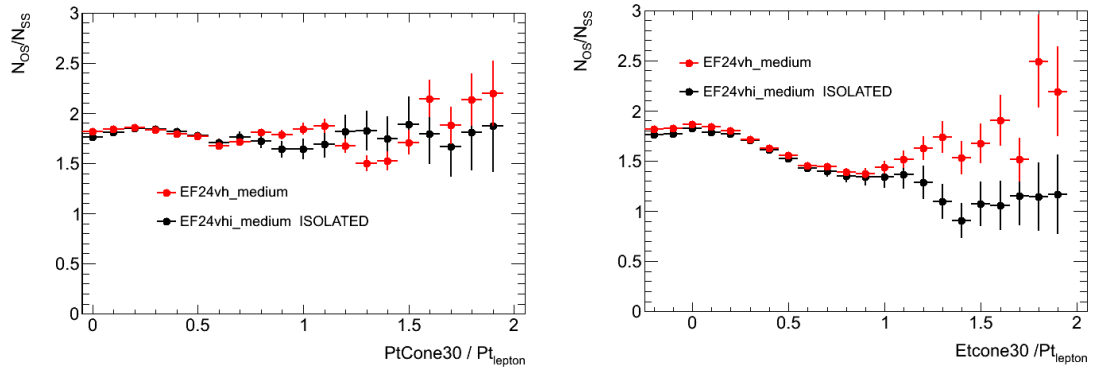
Figure A.2: R_{QCD} as a function of (a) $p_T(\mathrm{cone})$ / p_t and (b) $E_T(\mathrm{cone})$ /PT for the electron triggers with and without isolation requirement.

Appendix B

QCD Additional Plots
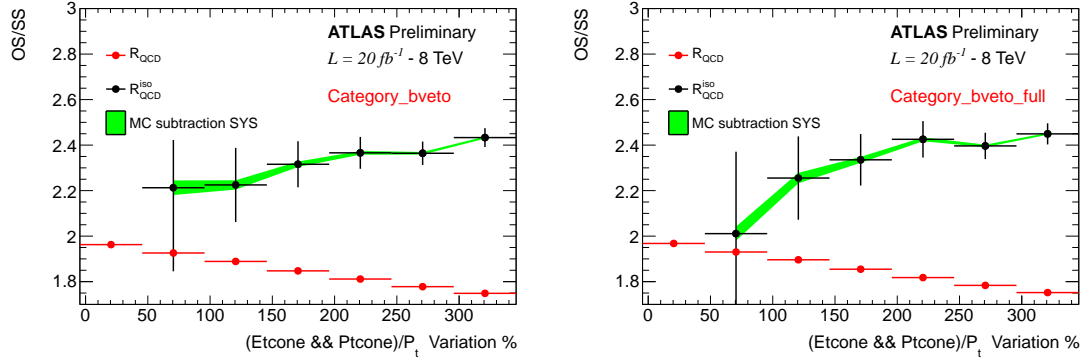
Figure B.1: OS/SS ratio as a function of lepton isolation variable selections (a) after the requirement of zero b-jets and (b) for the full b-veto selection. The isolation selections are varied as a percentage relative to the standard lepton isolation cut values (0 in the plot). The red points show the anti-isolated scale factor R_{QCD}, i.e. the ratio between regions C and D. The black points show the isolated SF, which is defined as the ratio between region $\hat{A}$ and $\hat{B}$, where the leptons have isolation values larger than the nominal value but smaller than the sliding cut.
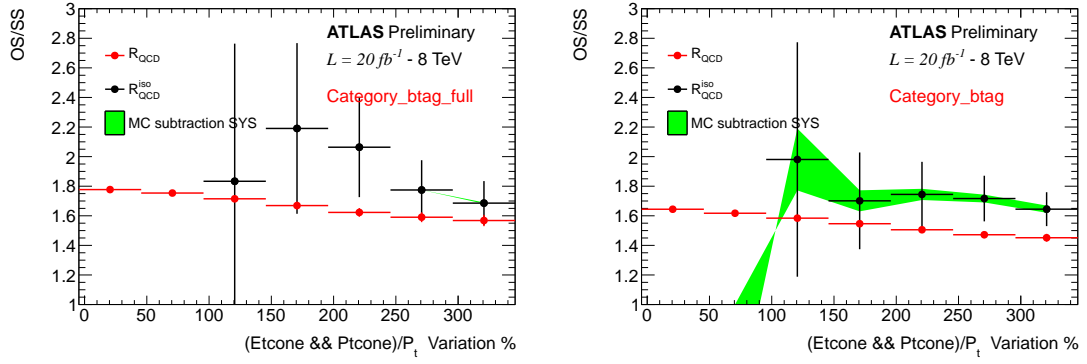
Figure B.2: OS/SS ratio as a function of lepton isolation variable selections (a) after the requirement of one b-jet and (b) for the full b-tag selection. The isolation selections are varied as a percentage relative to the standard lepton isolation cut values (0 in the plot). The red points show the anti-isolated scale factor R_{QCD}, i.e. the ratio between regions C and D. The black points show the isolated SF, which is defined as the ratio between region $\hat{A}$ and $\hat{B}$, where the leptons have isolation values larger than the nominal value but smaller than the sliding cut.

Appendix C

Limits cross checks and additional plots

During the limit derivation, the systematic uncertainties (translated in term of nuisance parameter) are fitted to the data, several checks are have been performed to ensure the quality of our statistical model. If some of the nuisance parameters are significantly different from their nominal value (ie before fit), it can be symptomatic of an important mis-modelling and must be carefully scrutinised. Also the correlation between the nuisance parameter and the signal strength (which reflects the degeneracy of the fit) is an important element to keep under control, in fact it reflects how well the data can constraint the nuisance parameters. Finally, to have a feeling of the behaviour of the likelihood at its minimum one can check the negative log likelihood profile in each nuisance parameter direction. We performed all this checks using the package NuisanceCheck-00-00-05 described in [73].

The signal and background model with the signal normalisation free (unconditional fit) is fitted to the data, in the following example plots the signal is assumed for the mass point mA = 120 GeV, $\tan\beta$ = 20, The difference between the post fit and pre-fit value of the nuisance parameter along with their errors is shown in figure C.1-C.3, respectively for the b-veto, b-tag channel and the combination between them. Figure C.4-C.6 shows the correlation matrix between the nuisance parameters respectively for the veto category, tag category and the combination between the two channels. Figure C.7-C.9 shows the behaviour of the likelihood at its minimum for each of the nuisance parameters (while a nuisance parameter is investigated the other are kept constant) for the combination between the channels.
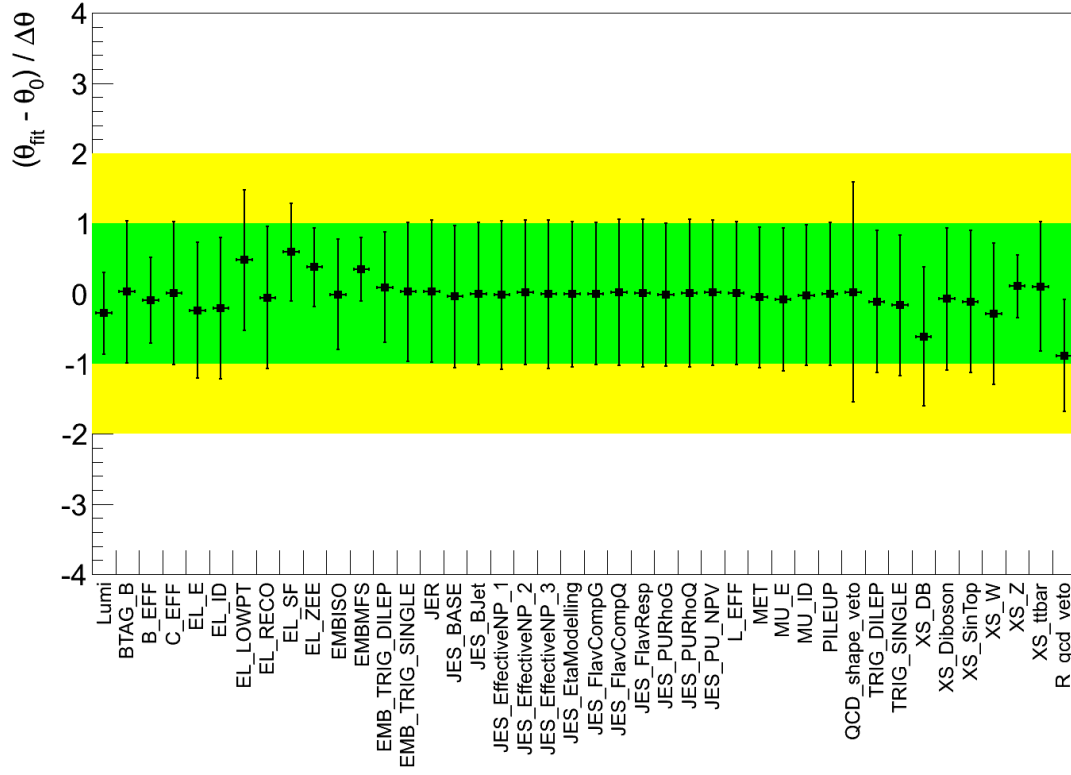
Figure C.1: Pulls for nuisance parameter considered in the fit, mA = 120 GeV, tanβ = 20, for the veto channel.
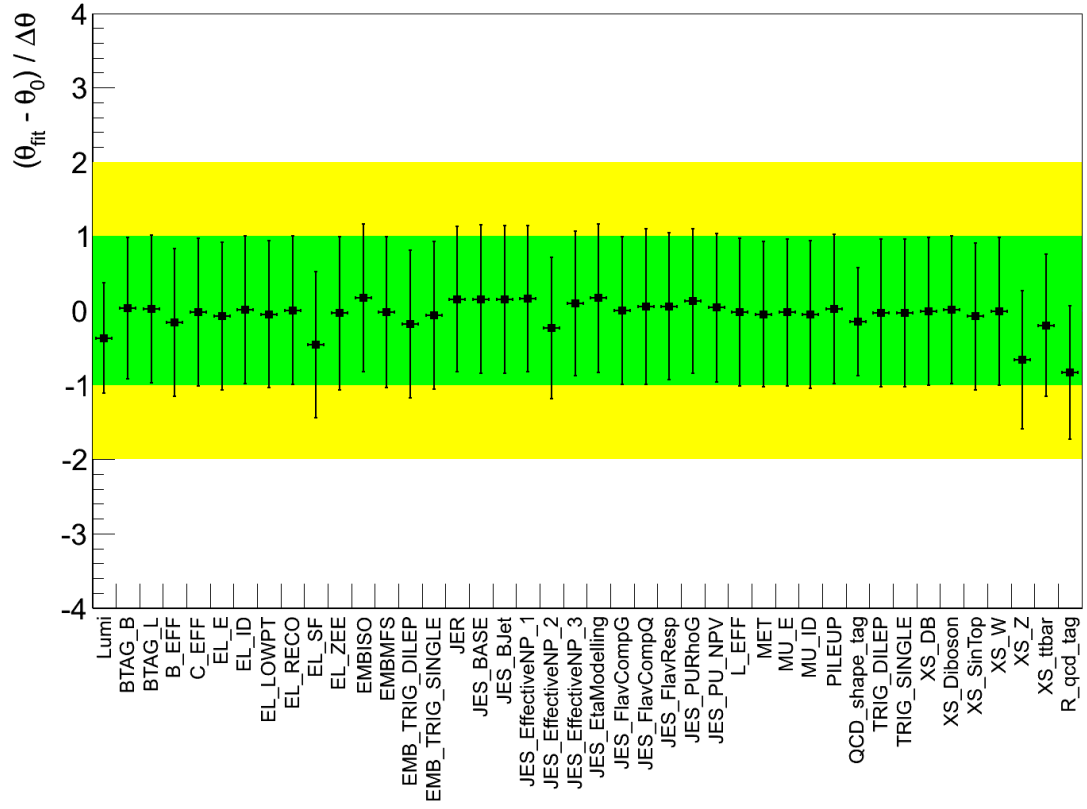
Figure C.2: Pulls for nuisance parameter considered in the fit, mA = 120 GeV, $\tan\beta = 20$, for the tag channel.
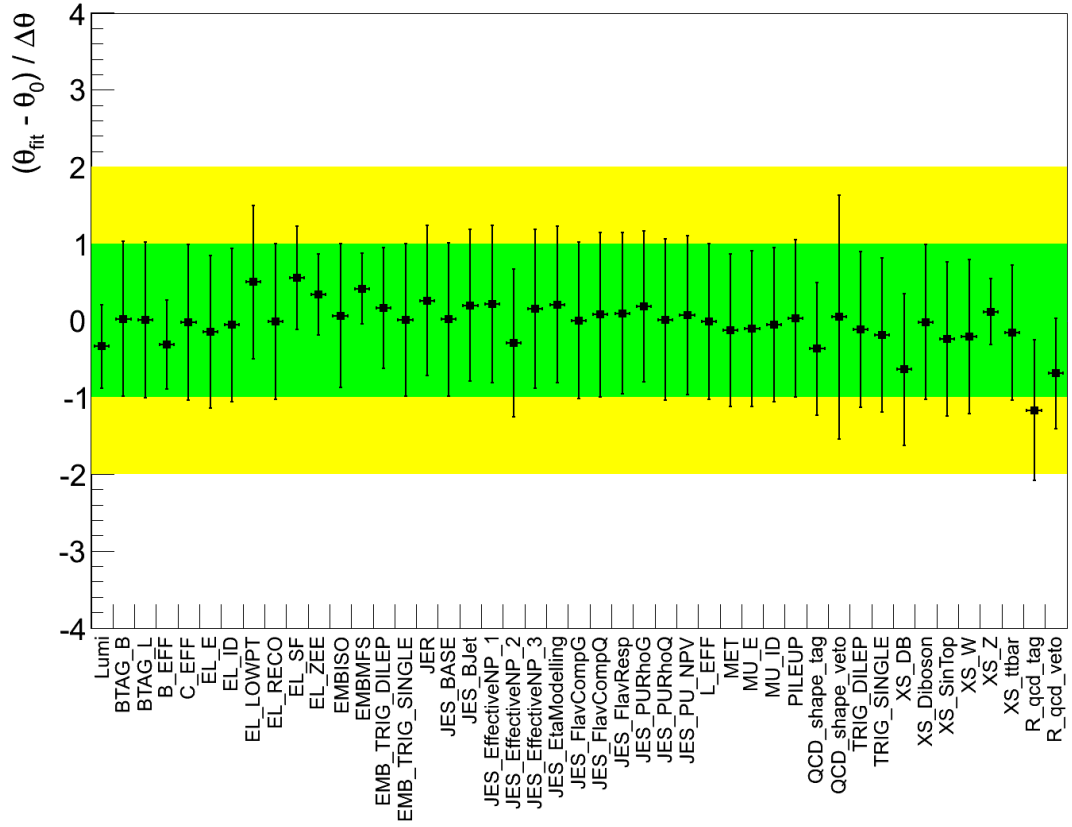
Figure C.3:   Pulls for nuisance parameter considered in the fit, mA = 120 GeV, $\tan\beta = 20$, combination between the two channel.
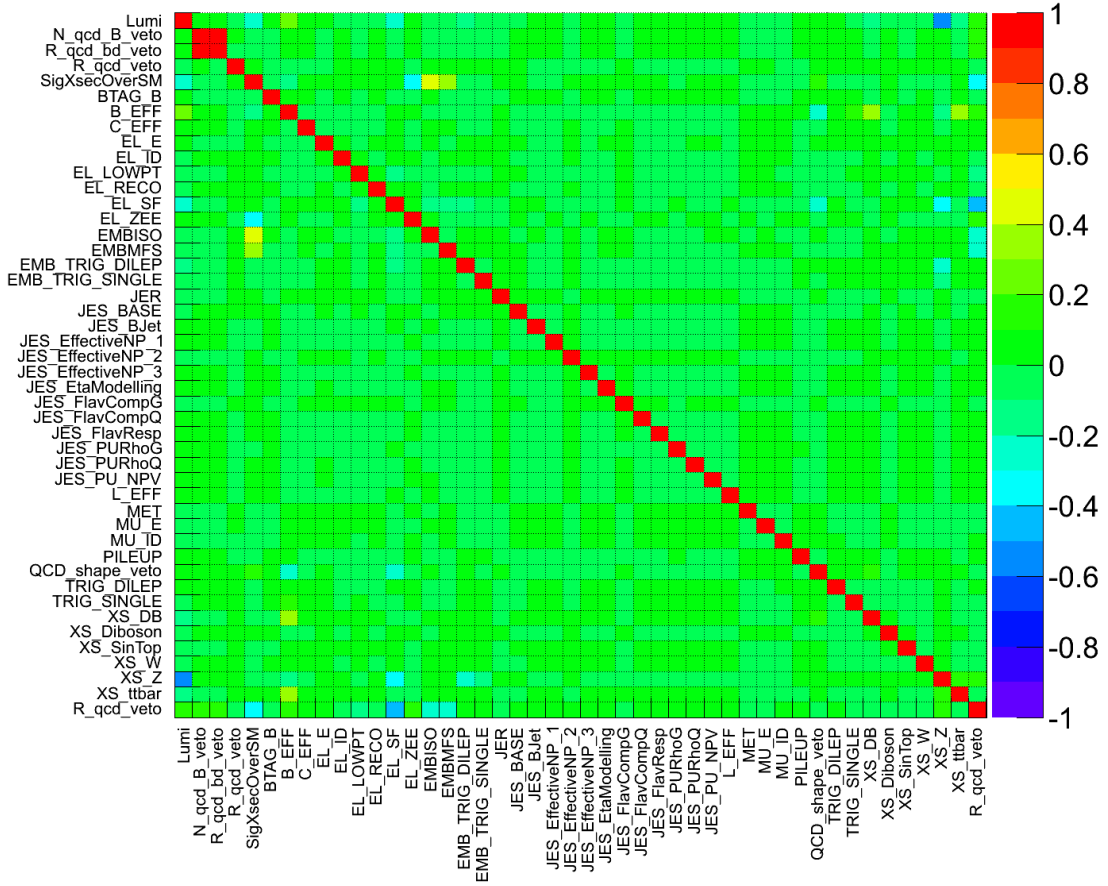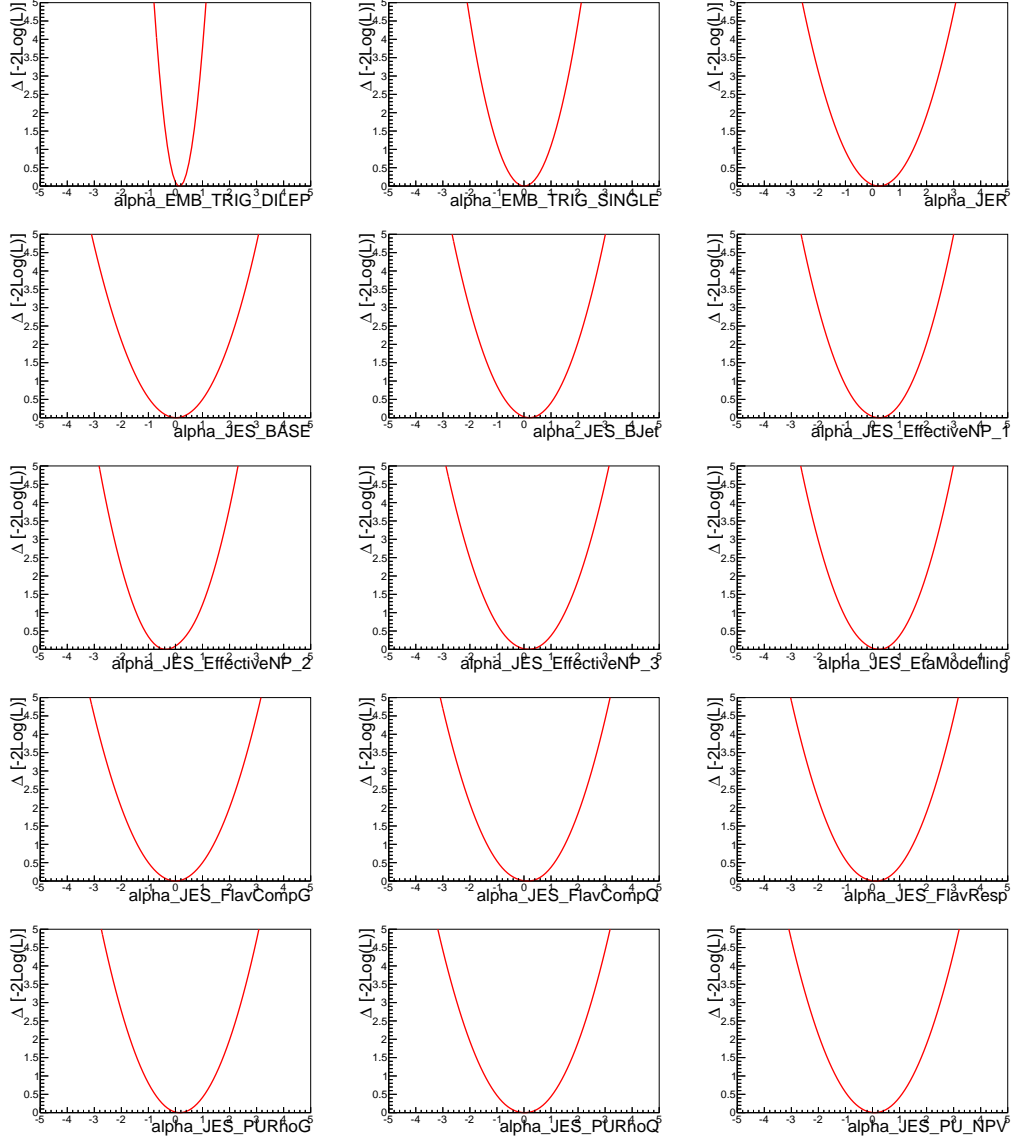
Figure C.4: Correlation matrix for nuisance parameters considered in the fit. The point mA = 120 GeV and tanβ = 20 is considered for the tag channel.

Figure C.5: Correlation matrix for nuisance parameters considered in the fit. The point mA = 120 GeV and tanβ = 20 is considered for the tag channel.

Figure C.6: Correlation matrix for nuisance parameters considered in the fit. The point mA = 120 GeV and $\tan\beta = 20$ is considered for the combination of the b-tag and b-veto channels.
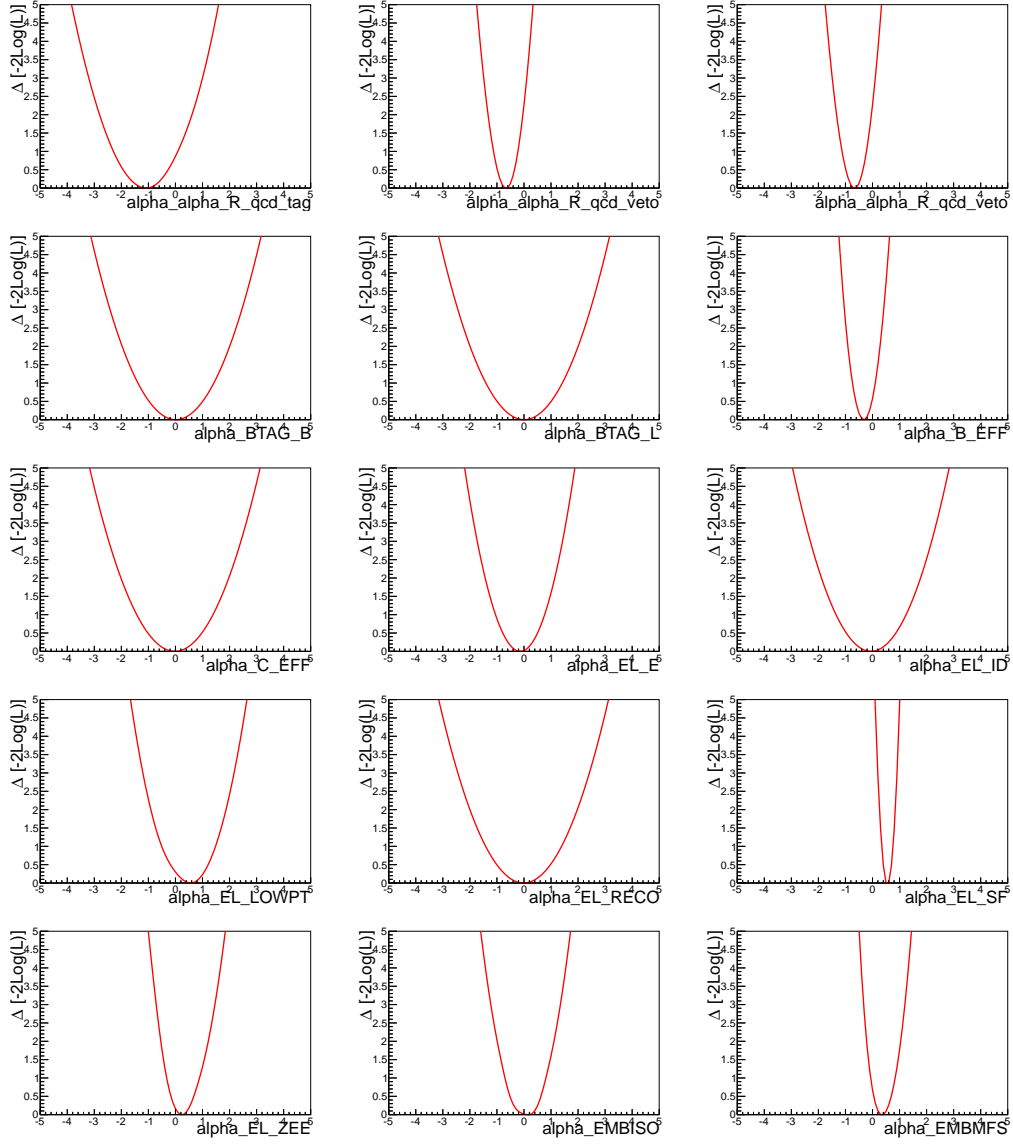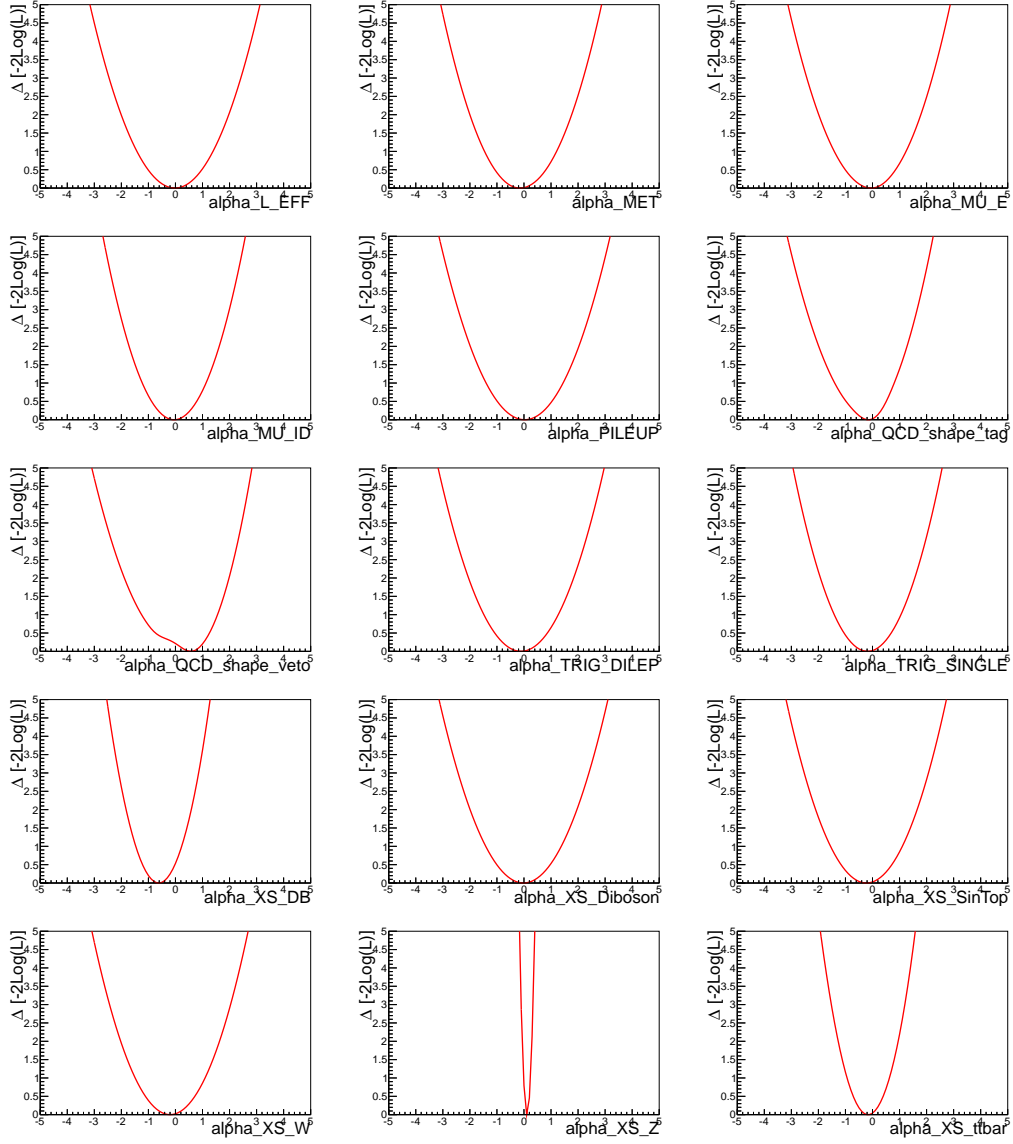
Figure C.7:   Likelihood scans for nuisance parameter considered in the fit, mA = 120 GeV, tanβ = 20, combination between the two channel.
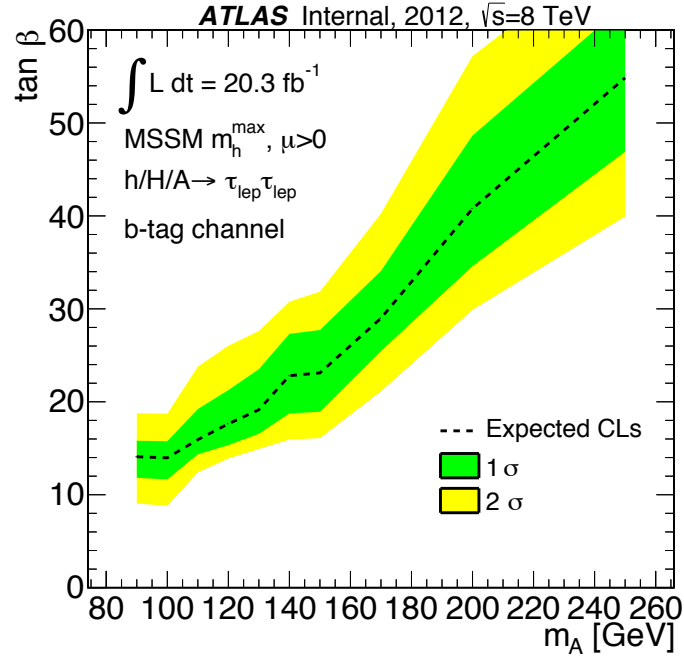
Figure C.8: Likelihood scans for nuisance parameter considered in the fit, mA = 120 GeV, tanβ = 20, combination between the two channel.

Figure C.9:   Likelihood scans for nuisance parameter considered in the fit, mA = 120 GeV, tanβ = 20, combination between the two channel.

Figure C.10: Expected exclusion limits, using the b-tag channel, for MSSM Higgs boson production in the MSSM m_A vs $\tan\beta$ parameter space.
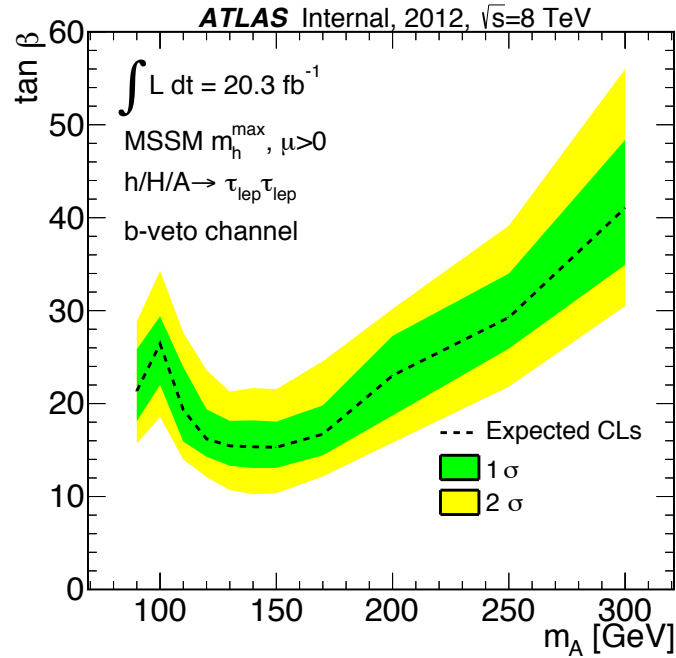

Figure C.11: Expected exclusion limits, using the b-veto channel, for MSSM Higgs boson production in the MSSM m_A vs $\tan\beta$ parameter space.
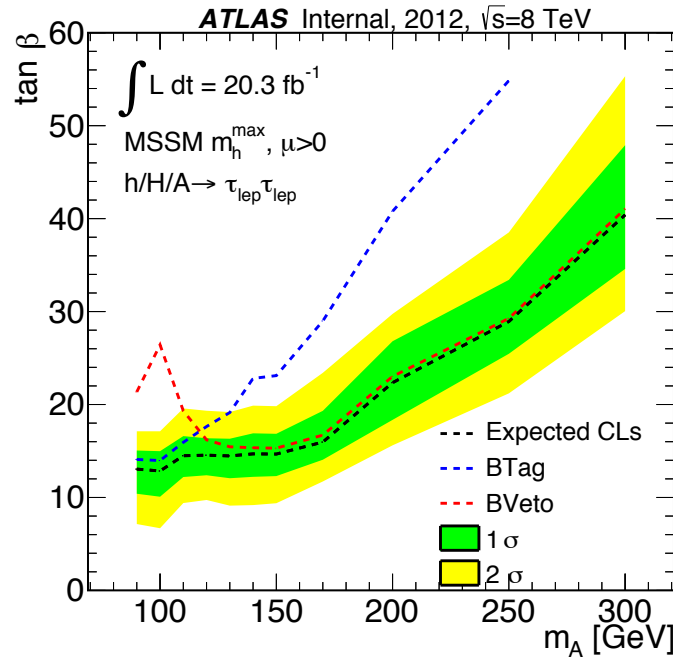
Figure C.12: Expected exclusion limits for MSSM Higgs boson production in the MSSM m_A vs $\tan\beta$ parameter space. Limits are compared for the b-tag and b-veto channel with the combined limit from both channels.